DOI:
10.1161/ATVBAHA.119.312732

Document Version
Peer reviewed version

URL: https://atvb-submit.aha-journals.org

Manuscript Number: ATVB/2019/312732R2

Title: Single-cell RNA-sequencing and Metabolomics Analyses Reveal the Contribution of Perivascular Adipose Tissue Stem Cells to Vascular Remodeling

Authors: Wenduo Gu (King's College London BHF Centre), Witold Nowak (King's College London BHF Centre), Yao Xie (Zhejiang University, School of Medicine,2nd Affiliated Hospital), Alexandra Le Bras (King's College London), Yanhua Hu (King's College London BHF Centre), Jiacheng Deng (King's College London BHF Centre), Shirin Issa Bhaloo (King's College London BHF Centre), Yao Lu (Center of Clinical Pharmacology, the Third Xiangya hospital, Central South University), Hong Yuan (The Third Xiangya Hospital, Central South University), Alka Saxena (King's College London), Tokuwa Kanno (King's College London), A. James Mason (King's College London), Jozef Dulak (Faculty of Biochemistry, Biophysics and Biotechnology, Jagiellonian University), Jingjing Cai (The Third Xiangya Hospital, Central South University), and Qingbo Xu (King's College London BHF Centre)

Single-cell RNA-sequencing and Metabolomics Analyses Reveal the Contribution of Perivascular Adipose Tissue Stem Cells to Vascular Remodeling

Wenduo Gu, PhD*[1], Witold N. Nowak, PhD*[1], Yao Xie, PhD*[1], Alexandra Le Bras, PhD[1], Yanhua Hu, MD, PhD[1], Jiacheng Deng, PhD[1], Shirin Issa Bhaloo, PhD[1], Yao Lu, MD[2], Hong Yuan, MD[2], Efthymios Fidanis, PhD[3], Alka Saxena, PhD[3], Tokuwa Kanno, PhD[4], A. James Mason, PhD[4], Jozef Dulak, PhD[5], Jingjing Cai, MD**[2] and Qingbo Xu, MD, PhD**[1]

[1]School of Cardiovascular Medicine and Sciences, King's College London, BHF Centre, London, United Kingdom (W.G., W.N.N., Y.X., A.L.B., Y.H., J.De., S.I.B., Q.X.);

[2]Center of Clinical Pharmacology, Department of Cardiology, Third Xiangya Hospital, Central South University, Changsha, China (Y.L., H.Y., J.C.);

[3]Genomics Research Platform, Biomedical Research Centre at Guy's Hospital, 7th Floor Tower Wing, Guy's Hospital, Great Maze Pond Road, London SE19RT, UK (E.F., A.S.);

[4]Institute of Pharmaceutical Science, School of Cancer & Pharmaceutical Science, King's College London, Franklin-Wilkins Building, London, UK (T.K., A.J.M.);

[5]Department of Medical Biotechnology, Faculty of Biochemistry, Biophysics and Biotechnology, Jagiellonian University, Kraków, Poland (J.Du.).

*Co-first authors

**Corresponding authors

Running title: Perivascular stem cells and vascular remodeling

Correspondence to:

Qingbo Xu, M.D., Ph.D.,

School of Cardiovascular Medicine & Sciences

King's College London BHF Centre

125 Coldharbour Lane

London SE5 9NU, United Kingdom

Telephone: (+44) 20 7848-5322

Email: qingbo.xu@kcl.ac.uk

Jingjing Cai, M.D.

Department of Cardiology

Third Xiangya Hospital

Central South University

138 Tong-Zi-Po Road, Changsha

Hunan 410013, China

Telephone: +86-15111133759

E-mail: caijingjing83@hotmail.com

Nonstandard Abbreviations and Acronyms:

ACTA2	smooth muscle α actin
ADSCs	adipose tissue-derived mesenchymal stem cells
αMEM	minimal essential medium
CNN1	calponin
Crat	carnitine acetyltransferase
DAPI	4′,6-diamidino-2-phenylindole
ECAR	extracellular acidification rate
ECs	endothelial cells
FABP4	fatty acid binding protein 4
FCCP	carbonyl cyanide-p-trifluoromethoxyphenylhydrazone
GC-MS	gas chromatography-mass spectrometry
MCP1	monocyte chemoattractant protein 1
GO	gene ontology
MDS	multi-dimensional scaling analysis
miR	microRNA
MSC	mesenchymal stem/stromal cells
NMR	nuclear magnetic resonance
OCR	oxygen consumption rate
OPN	osteopontin
PPARg	peroxisome proliferator-activated receptor-γ
PV-ADSCs	perivascular adipose tissue-derived mesenchymal stem cells
PVAT	perivascular adipose tissue
Q-PCR	quantitative-polymerase chain reaction
RFP	red fluorescent protein
Sca1	stem cell antigen 1
scRNA-seq	single-cell RNA-sequencing
SMCs	smooth muscle cells
SRC	spare respiratory capacity
TAGLN	smooth muscle protein 22-alpha
TCA cycle	tricarboxylic acid cycle
TGFb1	transforming growth factor β 1
TMRM	Tetramethylrhodamine, Methyl ester, Perchlorate

Abstract

***Objective*—**Perivascular adipose tissue (PVAT) plays a vital role in maintaining vascular homeostasis. However, most studies ascribed the function of PVAT in vascular remodeling to adipokines secreted by the perivascular adipocytes. Whether mesenchymal stem cells (MSCs) exist in PVAT and play a role in vascular regeneration remain unknown.

***Approach and Results*—**Single-cell RNA-sequencing (scRNA-seq) allowed direct visualization of the heterogeneous perivascular adipose tissue-derived mesenchymal stem cells (PV-ADSCs) at a high resolution and revealed two distinct sub-populations, among which one featured signaling pathways crucial for smooth muscle differentiation. Pseudotime analysis of cultured PV-ADSCs unraveled their smooth muscle differentiation trajectory. Transplantation of cultured PV-ADSCs in mouse vein graft model suggested the contribution of PV-ADSCs to vascular remodeling through smooth muscle differentiation. Mechanistically, treatment with TGFb1 and transfection of miR-378a-3p mimics induced a similar metabolic reprogramming of PV-ADSCs, including upregulated mitochondrial potential and altered lipid levels such as increased cholesterol and promoted smooth muscle differentiation.

***Conclusions*—**ScRNA-seq allows direct visualization of PV-ADSC heterogeneity at a single-cell level and uncovers two sub-populations with distinct signature genes and signaling pathways. The function of PVAT in vascular regeneration are partly attributed to PV-ADSCs and their differentiation towards smooth muscle lineage. Mechanistic study presents miR-378a-3p which is a potent regulator of metabolic reprogramming as a potential therapeutic target for vascular regeneration.

***Keywords*:** Perivascular adipose tissue, stem cells, single-cell RNA-sequencing, smooth muscle differentiation, vascular remodeling, metabolic reprogramming

Introduction

Perivascular adipose tissue (PVAT) anatomically abuts the adventitial side of the artery.[1] Changes in the phenotype of PVAT correlates with disease progression such as atherosclerosis, and the increase of volume and upregulation of inflammatory factors secreted by adipocytes are associated with worse outcomes.[2] Loss of PVAT resulting from the specific deletion of peroxisome proliferator-activated receptor-γ (PPARg) in murine smooth muscle cells (SMCs) contributes to endothelial dysfunction and impairs vascular homeostasis.[3] Moreover, transplantation of PVAT to the adventitia side of femoral artery after de-endothelialization injury accelerates neointimal hyperplasia.[4] However, most studies have attributed the function of PVAT to cytokines such as monocyte chemoattractant protein 1 (MCP1), and little is known about the possible impact of stem cells in the PVAT surrounding the vascular wall.[3, 4]

Tissue-resident stem cells, including vascular progenitors, are responsible for tissue remodeling.[5, 6] Adventitial stem/progenitor cells participate in vascular remodeling through migration towards the injury site and differentiation towards vascular lineages including SMCs.[7] Adipose tissue-derived mesenchymal stem/stromal cells (ADSCs) from the subcutaneous and visceral fat display the potential to differentiate towards vascular lineages including endothelial cells (ECs) and smooth muscle cells (SMCs).[8, 9] Therefore, it remains to be explored whether perivascular adipose tissue-derived mesenchymal stem cells (PV-ADSCs) exist in the PVAT and contribute to vascular remodeling through vascular lineage differentiation *in vivo* like adventitial stem/progenitor cells.

Mesenchymal stem cells (MSCs) from different tissues origins display similar phenotypic characteristics and multi-lineage differentiation potential *in vitro*, however, their well-documented heterogeneity has hindered major research progress in the field. Single-cell RNA-sequencing (scRNA-seq) analysis allows transcriptome profiling at the single-cell level and might help to gain further insight about distinctive sub-populations.[10] Recent studies have shown that metabolism which primarily sustains the energy need of stem cells regulates pluripotency and differentiation.[11] For example, fatty acid oxidation was found to be important for hematopoietic stem cell maintenance.[12] To date, whether the induction of SMC differentiation by TGFb1 is in part due to the metabolic regulation has not been investigated.

In this study, we demonstrate the heterogeneity of PV-ADSCs at a single-cell level and uncover two distinct clusters with specific signature markers and signaling pathways. Next, we show that PV-ADSCs participate in vascular remodeling *in vivo* notably through SMC differentiation. In addition, we demonstrate that during the SMC differentiation of PV-ADSCs, TGFb1 and miR-378a-3p induce a metabolic reprogramming consisting of increased mitochondrial oxidative metabolism, upregulated mitochondrial potential and altered lipid levels such as increased cholesterol level. Therefore, our study highlights the heterogeneity of PV-ADSCs at the single-cell level, unravels their importance in vascular remodeling and presents miR-378a-3p as a potential therapeutic target to prevent pathological vascular remodeling.

Materials and Methods

The data that support the findings of this study are available from the corresponding author upon reasonable request. Detailed materials and methods are in the online-only Data Supplement.

Experimental Mice

All animal procedures were approved by the UK Home Office. C57BL/6J mice were purchased from The Jackson Laboratory. Male mice aged 8-10 weeks were selected for surgery. Only male mice were selected for minimization of data variation brought by difference of sex. Breeding pairs of miR-378a-knockout mice (129SvEv/C57BL/6/mir-378-KO) were kindly provided by Dr. Eric Olson (University Texas Southwestern Medical Centre, Dallas, USA) and crossed with C57Bl/10ScSn-Dmdmdx/J mice for testing miR-378a effects in Duchenne muscular dystrophy (other work, in preparation). Protocols from the Institutional Committee for Use and Care of Laboratory Animal and license issued by Home Office UK were followed in all animal procedures.

Primary Culture of Adipose Tissue-derived Stem Cells from Mouse

Peri-aorta adipose tissues surrounding thoracic aorta (from the aortic arch to the aortic hiatus) of five 8-week-old C57BL/6J mice were pooled for each primary culture. Finely minced adipose tissue was washed with PBS once and then digested with 2 mg/ml Collagenase type I (Life Tech, 17018-029) for 30 min at 37°C in a shaker with a speed set at 100 rpm. The pellet was resuspended in stem cell culture medium [αMEM with 15% Embryomax (Millipore, ES-009-B), 0.1mmol/L 2-mercaptoethanol (Sigma), 10 ng/ml recombinant human leukemia inhibitory factor (Chemicon, Temecula, CA), 5ng/ml bFGF (R&D systems), 2 mmol/L L-glutamine (Sigma), 100 U/ml penicillin, and 100 mg/ml streptomycin (GIBCO, Grand Island, NY)] and placed in a 5% CO2 incubator. ADSCs from miR-378a knockout mice were isolated from the inguinal subcutaneous adipose tissue and cultured in the same manner. Cells within 10 passages were used.

Phenotyping of Primary and Cultured PV-ADSC

Primary cells obtained after the enzymatic digestion of peri-aorta adipose tissue or cultured cells detached with scraptase (GenDEPOT) were stained for 30 minutes at 4 °C with following antibodies: anti-CD45-APC (BD Biosciences, 561018), anti-CD29-PE (BD Biosciences, 562801), anti-Sca-1-PE-Cy7 (Biolegend, 108113), anti-CD31-PerCP (Biolegend, 201419), anti-CDH5-Alexa Fluor 647 (BD Biosciences, 562242), anti-PDGFRa-APC (eBioscience, 17-1401-81), anti-CD117-PE (Biolegend, 105807), anti-CD34-APC (Biolegend, 128611), anti-CD44-PerCP (Biolegend, 103035) and anti-CD11b-PE (Biolegend, 101205). Nucleated cells were distinguished from debris with Syto16 (Molecular Probes, S7578) and dead cells with DAPI. Cells were analyzed with BD Accuri C6 or BD LSR Fortessa II (both Becton Dickinson). Gating was set with appropriate fluorescence minus one controls or corresponding IgG controls.

Sorting and scRNA-seq of PV-ADSCs

Peri-aorta adipose tissue surrounding thoracic aorta (from the aortic arch to the aortic hiatus) was enzymatically digested to obtain primary PV-ADSCs. The cell suspensions were stained with Syto16, DAPI, CD45, CDH5, CD29, and Sca1 as described earlier in the phenotyping of primary and cultured PV-ADSCs. After proper gating, the single $Syto16^{+}$/$DAPI^{-}$/$CD45^{-}$/$CDH5^{-}$/$CD29^{+}$/$Sca1^{+}$ population were taken for subsequent scRNA-seq. RNA libraries were prepared on the contactless liquid handling system Labcyte Echo 525 (Labcyte Inc). Data quality was assessed with FastQC, reads were aligned to mouse genome (mm9) with HiSat2 2.0.5, sorted with SamTools 1.4 and assembled with StringTie 1.3.3.[13] R package scater was used for quality control (85 out of 94 cells with aligned reads greater than 800,000 were selected for further analysis) and normalization (default scaling normalization).[14] Automated Single-cell Analysis Pipeline (ASAP) with log-transformed and normalized values as input was used for multi-dimensional scaling (MDS), clustering, differential expression (DE method: SCDE).[15] Heatmaps and violoin plots of scRNA-seq data were plotted with R package ggplot2. Gene ontology (GO) and KEGG pathway analysis were performed with DAVID website.[16] Gene set enrichment analysis was carried out with GSEA software.[17]

For scRNA-seq of cultured PV-ADSCs, enzymatically digested cells that attached to the flask surface after 3 days (in αMEM with 10% FBS) and reached 80% confluency were dissociated and encapsulated in a gel bead and loaded to GemCode Instrument (10X Genomics) which generated barcoded single-cell droplets. Sequencing was carried out with standard protocol using 10X Single Cell 3' v2 and 10X chromium system. The library was sequenced with Nova PE150. In total, 12,158 cells were sequenced in one run. R package Seurat (version 2.3.0)[18] was leveraged for subsequent quality control and clustering analysis. Cells expressing <200 or >5000 genes were filtered out for exclusion of noncell or cell aggregates. Cells with a percentage of mitochondrial genes >0.05 were also filtered out. After quality control, 11,878 cells were included in subsequent analysis. After log-normalizing the data, principle component analysis was performed for dimension reduction. Clusters generated with the first 10 principal components were visualized with t-distributed stochastic nearest neighbor embedding. Expression of selected genes was plotted with Seurat function FeaturePlot.

Adult subcutaneous adipose tissue stromal vascular cells in published datasets (GSM3717978[19] and E-MTAB-6677[20]) were analyzed with corresponding methods described in the literature. Clustering-

specific markers for each mesenchymal stem cell population were found with MSC population subseted Seurat (version 3) object.

Pseudotime Trajectory Analysis

Pseudotime trajectory was plotted with R package monocle version 2.4 with default settings. Pseudotime ordering was performed using function reduceDimension with max_components set at 2 and reduction_method set as DDRTree. Cells that express *Acta2* but don't express *Myl6*, *Cnn1* or *Myh11* were set as starting point of pseudotime. Significant genes are obtained with function differentialGeneTest (fullModelFormulaStr = "~Pseudotime") and plotted with function plot_pseudotime_heatmap (num_clusters = 3). In the heatmap, predicted values generated by function genSmoothCurves were plotted along 100 evenly spaced pseudotime values.[21] Genes included in KEGG term TGFb signaling or transcription factors (list obtained from transcription factor database[22]) were intersected with the 3 significantly changed gene modules and presented as heatmap. Branch point analysis was performed with BEAM function.

Smooth Muscle Differentiation

PV-ADSCs were seeded on gelatin-coated flasks and differentiated with medium [αMEM with 10% FBS and 5 ng/ml TGFb1 (R&D systems)] for indicated time. Leptin (Peprotech, 450-31) or IGFBP2 (R&D Systems, 797-B2-025) at indicated concentrations were used to manipulate differentiation.

RFP Labeling of Cells

Lentiviral particles used to label PV-ADSCs with RFP were generated with LV H2b_RFP plasmid[23] (a gift from Elaine Fuchs, Addgene, 26001).

Subcutaneous Matrigel plug assay

Subcutaneous *Matrigel* plug assay experiments were conducted as described.[6, 24, 25] PV-ADSCs were differentiated for 5 days with αMEM with 10% FBS 5 ng/ml TGFb1. Mouse MS1 ECs (ATCC, CRL-2279) were prepared. Differentiated PV-ADSCs and mouse ECs were mixed in a 1:1 ratio in 100 µl *Matrigel* and injected subcutaneously to mice. The plugs were harvested 14 days after the injection for immunostaining and H&E staining. To track the PV-ADSCs, RFP-labeled cells were used.

Cell Transplantation

Mouse vein segments were iso-grafted into carotid arteries of C57BL/6J mice.[26] RFP-labeled PV-ADSCs in culture (10^6 cells) were seeded onto the adventitial side to envelope the vein grafts. Vein graft transplantation without cell wrapping was used as control. Grafted tissue fragments were harvested 2 weeks post-surgery and stained with H&E and immunofluorescent markers.

^{1}H NMR (nuclear magnetic resonance) metabolomics analysis

Undifferentiated ADSCs and ADSCs cultured in differentiation medium (αMEM with 10% FBS and 5 ng/ml TGFb1) for 1 day were harvested and frozen in liquid nitrogen. Eight samples were acquired in each treatment and ^{1}H NMR metabolomics was carried out using method published with modifications.[27]

GC-MS (Gas Chromatography – Mass Spectrometry) metabolomics analysis

Undifferentiated ADSCs, ADSCs differentiated for 4 days, cells treated with miRNA mimic negative control or miR-378a-3p mimics were harvested, frozen in liquid nitrogen before analysis. Extraction of metabolites were done using a published protocol with modification.[28]

Metabolomics Data Processing

Annotated metabolites and correspondent abundance were normalized to the total level of metabolites. Data scaling was mean-centered and divided by standard deviation of each variable. Orthogonal projection to latent structures analysis[29] and heatmap of various metabolites were obtained from MetaboAnalyst software.[30]

Transfection of miRNA mimics, miRNA inhibitors and siRNAs

PV-ADSCs with 70% confluence were transfected with miRNA mimics, inhibitors or siRNAs (Thermo Fisher) with Lipofectamine RNAiMAX (Thermo Fisher). After optimization, the concentrations of miRNA mimics, miRNA inhibitors and siRNAs were respectively 12.5, 60 and 12.5 nmol/L.

Oxygen consumption rate and extracellular acidification rate measurements

Oxygen consumption rate and extracellular acidification rate are measured with the Seahorse XF-24 extracellular flux analyzer (Seahorse Bioscience). PV-ADSCs with indicated treatments and corresponding controls were plated on XF24 microplate coated with gelatin one day prior to the assay. XF Cell Mito Stress Kit was used to study the mitochondrial metabolism. OCR and ECAR at basal level and after metabolic perturbations with the addition of 1 μmol/L oligomycin, 1 μmol/L carbonyl cyanide-p-trifluoromethoxyphenylhydrazone (FCCP) and 1 μmol/L rotenone and antimycin A were measured. Calculations were obtained with the Agilent Seahorse Wave Software for Agilent Seahorse XF analyzers (Seahorse Bioscience).

Statistical Analysis

Data with 5 or more experiment repeats passed KS normality test that determines data normality and the *F*-test that assesses homogeneity of variance. Unpaired and two-tailed student's t test were applied to analyze data between two groups. Data were expressed as mean±SD (standard deviation) using GraphPad Prism 6. Comparisons across multiple groups with 5 experiment repeats per group were assessed with one-way ANOVA test, followed by Bonferroni post-hoc analysis. Comparisons across multiple groups with 3 experiment repeats per group were assessed with Kruskal-Wallis test, followed by Bonferroni post-hoc analysis. Experiment repeats in each group were specified in the figure legends. P value < 0.05 was considered statistically different.

Data Availability

Clustering result of primary PV-ADSC scRNAseq data has been made public on the ASAP website (https://asap.epfl.ch) with the project name PV-ADSC scRNAseq. Raw sequencing data of primary PV-ADSCs are available in Gene Expression Omnibus (GSE132581). Additional data are available from the corresponding author upon request.

Results

Characterization and Localization of Stem Cells in the Perivascular Adipose Tissue

MSCs exist in almost all organs of the body.[31] Adipose tissue-derived MSCs from the subcutaneous fat exhibit potential for tissue remodeling with multi-lineage differentiation capacities and immunomodulation effect.[32] Thus, we hypothesized that MSCs also reside in the PVAT. To examine this, the adipose tissue surrounding mouse thoracic aorta was enzymatically digested and cultured *in vitro*. In the isolated adipose tissue, similar coverage of PLIN1 (Perilipin1), an adipocyte marker with cell nucleus as well as minimal staining of PLIN1 in remaining adventitia confirms minimal contamination of adventitial cells (Figure I in the online-only Data Supplement), although slight contamination could not be excluded given the proximity of peri-aorta adipose tissue and adventitia. More than 95% of the cells express MSC marker CD29 and 73.55% ± 2.85% express mouse stem cell marker Sca1 (Figure 1A and 1B). CD34, which is also an MSC marker[33], displayed high expression in around 68.30% ± 2.70% of the cultured cells (Figure 1A and 1B). Furthermore, only 1~3% of the cells express hematopoietic marker CD45, macrophage marker CD11b, progenitor marker c-Kit, and endothelial marker PECAM1 (Figure 1A and 1B). In addition, around 63% of the cells expressed pericyte or fibroblast marker PDGFRa and more than 95% expressed CD44 (Figure IIA in the online-only Data Supplement). Furthermore, the cells isolated from the PVAT exhibited adipogenic and osteogenic differentiation capacities (Figure IIB-IIE in the online-only Data Supplement). Thus, in consistency with the *in vitro* definition of MSCs proposed by the International Society for Cellular Therapy[34], phenotypic analysis and multi-lineage differentiation capacities confirmed the existence of MSCs within the peri-aorta adipose tissue. These cells are referred to as PVAT-derived mesenchymal stem cells (PV-ADSCs) below.

After characterization of the phenotypic markers, the *in situ* localization of PV-ADSCs was studied. To exclude endothelial cells and adipocytes from the PV-ADSC population, staining of endothelial marker PECAM1 and adipocytes marker PLIN1 was performed. MSC marker CD29 was utilized because of its consistent and high expression in primary peri-aorta adipose tissue cells (Figure 2A) and cultured PV-ADSCs (Figure 1). As adventitial Sca-1^{+} cells play a crucial role in neointima formation and vascular pathogenesis[35], Sca-1 expression in CD29^{+}/PECAM1^{-}/PLIN1^{-} cells was examined. The results showed that PVAT contains a population of CD29^{+}/PLIN1^{-}/PECAM1^{-} cells and that some of the cells co-express Sca-1 (Figure 1C). To conclude, a CD29^{+}/Sca1^{+}/PLIN1^{-}/PECAM1^{-} PV-ADSC population was identified in the PVAT.

ScRNA-seq of PV-ADSCs Reveals Two Distinct Clusters

Heterogeneity has been a long-standing question in the research field of MSCs.[34] To achieve a high-resolution phenotyping of the PV-ADSCs, scRNA-seq was utilized. Among the enzymatically digested peri-aorta adipose tissue cells (freshly isolated cells without *in vitro* culture), single live cells were sorted for CD45^{-}/CDH5^{-} population to exclude the hematopoietic and endothelial lineages (Figure 2A). Subsequently, scRNA-seq was performed in CD29^{+}/Sca1^{+} cells (60.15% ± 3.17% in non-immune non-endothelial cells) (Figure 2A and Figure IIIA in the online-only Data Supplement). Selection of CD29 and Sca1 as the positive markers of PV-ADSCs was supported by our previous phenotypic and *in situ* characterization and previous publications.[20, 36] Interestingly, Dpp4^{+} interstitial progenitors in mouse subcutaneous inguinal white adipose tissue showed an enrichment of Sca1 compared to committed Icam1^{+} proadipocytes (Figure IIIB in the online-only Data Supplement), which further supported the use of Sca1 for enrichment of ADSCs.[19]

Among the 94 single cells captured, 85 cells with the number of aligned reads greater than 800,000 were selected for further analysis (Figure IIIC in the online-only Data Supplement). Two distinct clusters (cluster 1 and cluster 2) were identified which contained 30 and 55 cells respectively (Figure 2B). Cluster 2 featured the expression of *Tgfbr2*, an important component of TGF-beta signaling pathway (Figure 2C), whereas cluster 1 exclusively expressed *Pecam1* (Figure IIIH in the online-only Data Supplement), an endothelial marker and *Cd36* (Figure 2C and 2D), which is important for fatty acid uptake. The signature genes for cluster 1 and 2 were illustrated as a heatmap (Figure 2D). Important signaling pathways in cluster 1 included VEGF-activated receptor activity and PPAR signaling (Figure 2E). The feature signaling pathways for cluster 2 were those essential in smooth muscle differentiation such as PDGF binding, IGF binding, PI3K-Akt signaling and TGF-beta signaling (Figure 2F). Furthermore, gene sets of myogenesis and TGF-beta signaling presented a positive correlation with cluster 2 (Figure 2G). The results implied that cluster 1 cells display angiogenic potential, whereas cluster 2 cells demonstrate enriched expression of genes involving pathways that are important in SMC differentiation.

Single-cell level examination of MSC or pericyte markers including *Mcam*[31], *Tbx18*[37], *Cspg4*[31] and *Pdgfra*[36] *etc.* revealed substantial heterogeneity at a high resolution (Figure 2H). High expression of *Ly6a* was observed in both clusters, while other markers such as *Cd34*, *Cd44*, *Pdgfra* and *Pdgfrb* were mainly expressed in cluster 2 (Figure 2I). Heterogeneous expression of stemness markers such as *Klf4* and *Myc*[38] was also observed (Figure IIID in the online-only Data Supplement). Additionally, the cells in cluster 1 demonstrated exclusive expression of adipogenesis markers *Fabp4* and *Pparg* (Figure IIIE and IIIF in the online-only Data Supplement). Endothelial marker *Cdh5* was also mainly expressed in cluster 1 cells (Figure IIIG and IIIH in the online-only Data Supplement). No cell expressed SMC markers including *Cnn1*, *Tagln*, *Acta2* and *Myh11* (not shown). Interestingly, fibroblast markers such as *Vimentin* demonstrated heterogeneous expression in primary PV-ADSCs (Figure IV in the online-only Data Supplement). Relatively limited heterogeneity resulted from the relatively small number of cells analyzed was complimented by analysis of published datasets which offered clue of subcutaneous stromal vascular cell hierarchy (Figure V in the online-only Data Supplement).[19, 20] To conclude, scRNA-seq allowed unprecedented direct visualization of MSC heterogeneity, revealing two distinct clusters with discrete signature gene sets and signaling pathways. Multiple gene sets involved in SMC differentiation were enriched in cluster 2.

Pseudotime Analysis of Cultured PV-ADSCs Uncovers a SMC Differentiation Trajectory

While scRNA-seq of primary PV-ADSCs reflected their function and heterogeneity *in vivo*, further scRNA-seq of cultured PV-ADSCs offered an opportunity to examine a larger number of cells. In total, 12,158 cells were detected, with a median 2,602 genes per cell. After quality control by including cells with gene number between 200 and 5,000 and filtering out cells with fraction of mitochondrial genes higher than 0.05, 11,878 cells were leveraged for subsequent analysis (Figure VIA and VIB in the online-only Data Supplement). Consistent with our previous flow cytometry data (Figure 1A), cultured PV-ADSCs exhibited minimal level of *Cdh5* expression with only 0.48% of the cells positive for *Cdh5* (Figure VIC and VIE in the online-only Data Supplement). On the contrary, *Tgfbr2* and *Col3a1,* both marker genes of cluster 2 in primary PV-ADSCs, displayed high expression in cultured PV-ADSCs with 29.26% and 93.79% of the cells positive for these markers respectively (Figure VIC and VIE in the online-only Data Supplement). Interestingly, 6.23% of the cells expressed mature SMC marker *Myh11* (Figure VID and VIE in the online-only Data Supplement). Additionally, most of the 15 cluster 1 marker genes displayed expression in less than 5% cultured cells, whereas most of the cluster 2 marker genes were expressed in more than 25% of the cultured cells (Figure VIF in the online-only Data Supplement).

Pseudotime trajectory analysis was employed to inspect progression of continuous cell states. It is noted here that the trajectory here was not complimented by real differentiation time points and thus offers only suggestions of differentiation mechanism, which requires further experimental proof. Since the PV-ADSCs were kept in basal conditions without additional stimulation factor towards adipocytes or osteocytes, minimal expression of markers for these cell types were expressed (Figure VIIA in the online-only Data Supplement). Cultured PV-ADSCs displayed different level of *Acta2, Myl6, Cnn1* and *Myh11* expression (Figure 3A and Figure VIIB in the online-only Data Supplement). Pseudotime analysis ordered cells expressing different levels of SMC markers in a trajectory (Figure 3B). Mature SMCs (stage 4) was located towards the termini of the trajectory, which is partly a validation for the constructed trajectory (Figure 3C). Significantly changed genes along the pseudotime trajectory were assigned to three gene modules (Figure 3D). In the downregulated gene module were *Lpl* (Figure 3D), an enzyme important for lipid metabolism[39], stem cell marker *Ly6a* (Figure 3E) and fibroblast marker *Dcn* (Figure VIIB in the online-only Data Supplement). *Vim* and *Tpm3* were from gene module 2 and upregulated along the pseudotime, peaking in the middle of the trajectory (Figure 3D). SMC marker *Acta2*, pericyte marker *Mcam*, and MSC marker *Cd44* were in gene module 3, reaching highest expression towards the end of trajectory (Figure 3D). For the upregulated genes (gene module 2 and 3), essential pathways for SMC differentiation such as HDAC binding, histone binding, acting binding, IGF binding and TGFR binding were enriched (Figure 3F). In the TGF-b signaling pathway, the upregulation of *Tgfb1* (in gene module 2), *Rock2* and *Rhoa* (in gene module 3) along pseudotime trajectory further underlines the importance of this pathway in SMC differentiation (Figure 3G). In particular, *Tgfb2* and also the total level of significantly changed genes in TGF-b signaling were increased during differentiation (Figure 3H). Importantly, along the trajectory, *Cebpb*, which is crucial for adipogenesis, and *Runx1*, which drives osteocyte differentiation[40], decreased (Figure 3I). It is noted that pseudotime heatmap plots predicted values generated by function genSmoothCurve in monocle (version 2) along 100 evenly spaced pseudotime values rather than real expression values.[21] Cells located at the branches of the trajectory including states 8, 7, 5 and 9 demonstrated enriched expression of genes involved in GO terms antioxidant activity, laminin binding, hormone receptor binding and IL1 activity receptor binding respectively, which is consistent with the broad spectrum of function reported for mesenchymal stem cells such as immunomodulation (Figure VIII in the online-only Data Supplement).[41]

PV-ADSCs Participate in Vascular Remodeling in vivo and Differentiate towards SMCs in vitro

Both adventitial progenitors and PV-ADSCs are located close to the aorta, among which adventitial progenitors have been demonstrated to participate in vascular remodeling.[7] To better characterize PV-ADSCs, comparison of their single-cell level transcriptomic signature with adventitial mesenchyme cells (Adventitial Mesen I-IV clusters)[42] were performed. Cluster-defining genes for Adv-Mesen cells were enriched in cluster 2 cells of primary PV-ADSCs, with Mesen II cluster markers most highly expressed (Figure IXA in the online-only Data Supplement). Additionally, only cluster 2 markers were highly expressed in Adv-Mesen cells and their slight enrichment in Mesen II cluster was also

observed (Figure IXB in the online-only Data Supplement). Comparison of Sca1$^+$ (normalized expression > 1) cells from Adv-Mesen cells and cultured PV-ADSCs was further conducted. Interestingly, *Ccl2* (C-C motif chemokine ligand 2), which proved important for the pro-inflammatory function of adventitial Sca1$^+$ cells[42], was among the genes with high variation in both groups (Figure IXC from online-only Data Supplement). Various genes were differentially expressed in Sca1$^+$ Adv-Mesen cells and cultured PV-ADSCs, among which fibroblast marker *Dcn* (decorin) and actin filament regulating *Gsn* (gresolin) were enriched in Adv-Mesen cells, and *Timp1* (tissue inhibitor of metalloproteinases 1) and *S100a4* (S100 calcium binding protein A4) were highly expressed in cultured PV-ADSCs (Figure IXD and IXE in the online-only Data Supplement). In terms of pathway analysis, genes expressed higher in cultured PV-ADSCs displayed enrichment of GO terms actin binding and actin filament binding, whereas those selectively expressed in Adv-Mesen cells were enriched for GO term chemokine activity and antioxidant activity (Figure IXF in the online-only Data Supplement). However, it should be noted that cultured PV-ADSCs and primary Adv-Mesen cells were compared. Cell culture conditions might introduce transcriptomic difference. Collectively, cluster 2 PV-ADSCs displayed certain similarity with adventitial Sca1$^+$ cells, whereas transcriptomic difference was more prominent.

To explore whether PV-ADSCs participate in vascular remodeling *in vivo*, a vein graft model was used. Transplantation of cultured PV-ADSCs to the adventitia side of the vein graft significantly promoted the neointima formation (Figure 4A). RFP signal in the neointima area indicated the migration of the RFP-labeled PV-ADSCs from the adventitia side to the intima (Figure 4B). Numerous RFP positive cells expressed SMC marker ACTA2, implying that the contribution of PV-ADSCs to neointima formation might be partly through SMC differentiation (Figure 4B). Fibroblast marker Vimentin was also expressed in some RFP-positive cells (Figure XA in the online-only Data Supplement). Notably, no co-localization of RFP with macrophage marker CD68 was observed, suggesting that participation of PV-ADSCs in vascular remodeling was not through macrophage differentiation (Figure XB in the online-only Data Supplement).

After establishing that PV-ADSCs contribute to vascular remodeling partly through SMC differentiation *in vivo*, their potential to differentiate towards SMCs *in vitro* was next explored for subsequent mechanism study. TGFb1 was utilized as stimulus for differentiation, given the role of TGFb1 signaling in SMC differentiation implied by scRNA-seq. Upon treatment with TGFb1, PV-ADSCs differentiated towards SMCs, as displayed by the upregulation of SMC markers including Cnn1, Tagln and Acta2 at the mRNA and the protein level (Figure 4C-4E). Collagen gel contraction assay demonstrated better contractility of SMCs differentiated from PV-ADSCs (Figure XI in the online-only Data Supplement). Since brown adipose tissue has been gradually recognized as a secretory organ, we also checked the effect of IGFBP-2, an adipokine secreted predominantly by brown adipose tissue[43], on PV-ADSC differentiation towards SMCs. High concentration (250 ng/ml) IGFBP-2 promoted SMC differentiation with the presence of TGFb1, whereas no effect was observed for leptin, an adipokine secreted mainly by white adipose tissue (Figure XIIA and XIIB in the online-only Data Supplement). Interestingly, PV-ADSCs also expressed high level of IGFBP-2 in comparison with ADSCs isolated from subcutaneous adipose tissue (Figure XIIC in the online-only Data Supplement). Additionally, PV-ADSC migration towards chemoattractant SDF1 was also observed (Figure 4F), consistent with the notion that participation of PV-ADSCs *in vivo* involves complex processes including differentiation and migration.[7]

To further investigate the function of SMCs differentiated from PV-ADSCs, the cells were mixed with mouse MILE SVEN 1 ECs in *Matrigel* and then injected subcutaneously in wild-type mouse to check their ability to participate in vasculogenesis with the assistance of mature ECs. As exhibited by H&E staining of the subcutaneous *Matrigel* plug, a relatively large tube-like structure with multiple layers was formed in the plug with differentiated PV-ADSCs and ECs, whereas it was not found in control group (Figure 4G). Immunostaining of the *Matrigel* plug showed proximal localization of ACTA2 and PECAM1, demonstrating that the tube-like structure was a vessel (Figure 4H). Altogether, functional SMCs can be derived from PV-ADSCs.

Metabolic Reprogramming of PV-ADSCs during SMC Differentiation Induced by TGFb1

Metabolic reprogramming in stem cells not only helps to meet the energy requirement, but also drives various processes such as differentiation.[44] To investigate metabolic changes in the SMC differentiation of PV-ADSCs induced by TGFb1, NMR (nuclear magnetic resonance) metabolomics was firstly performed. Abundance of various detected metabolites demonstrated notable changes during differentiation (Figure 5A). Orthogonal projection to latent structures analysis depicted the distinct metabolic status of differentiated PV-ADSCs (Figure 5B). Functionally, cells treated with TGFb1 exhibited higher basal mitochondrial oxygen consumption rate (OCR), higher maximal mitochondrial OCR as well as stronger spare respiration capacity (SRC) (Figure 5C). Consistently, higher mitochondrial potential was detected in differentiated PV-ADSCs (Figure 5D). These results implied that the mitochondrial oxidative metabolism was enhanced during differentiation.

Further characterization of the metabolic change was examined with GC-MS metabolomics which is more sensitive and detects more metabolites. Enrichment of metabolites from tricarboxylic acid (TCA) cycle (Figure 5E) during differentiation indicated the increased mitochondrial activity, which was consistent with the upregulated OCR and mitochondrial potential. Fueled by the observation that mitochondrial activity was increased during differentiation, we postulated that the reactive oxygen species (ROS) might influence SMC differentiation. However, SMC markers were not altered by the treatment of H_2O_2 (Figure XIIIA in the online-only Data Supplement) or the transfection of *Nox4* siRNA (Figure XIIIB in the online-only Data Supplement) which changed the ROS level. Treatment of FCCP which potently uncoupled the electron transduction and oxidative phosphorylation also displayed only mild effect on SMC marker expression (Figure XIIIC in the online-only Data Supplement). Notably, as indicated by the increased phosphoenolpyruvate and lactate level (Figure XIIID in the online-only Data Supplement), glycolysis was also upregulated during differentiation. Functional characterization of glycolysis showed the upregulation of both the basal glycolysis and glycolysis capacity in cells treated with TGFb1 (Figure XIIIE in the online-only Data Supplement). However, glucose uptake did not show much change and glucose treatment did not have effect on the SMC marker expression (Figure XIIIF and XIIIG in the online-only Data Supplement).

More extensive examination of the GC-MS metabolomics data revealed the upregulation of various lipids in differentiated PV-ADSCs (Figure 5F). The increased lipid together with the more active mitochondria suggested a potential change of lipid metabolism. Significant changes in *Ppara, Pparg, Prdm16, Ucp1, Cebpb* and *Cebpd* were observed during SMC differentiation, supporting the hypothesis that lipid metabolism drastically reprogrammed during differentiation (Figure 5G). Changes of these markers along the trajectory and in real time further supported the reprogramming of lipid metabolism (Figure 5H and Figure XIV in the online-only Data Supplement). The change of various lipid levels led us to investigate the lipid oxidation process, which relies on the trans-mitochondrial transport of fatty acids regulated by carnitine acyltransferases including carnitine palmitoyltransferase 1 (*Cpt1*) and carnitine acetyltransferase (*Crat*).[45] *Cpt1* is responsible for the transport of long-chain fatty acids and *Crat* is responsible for the transport of short-chain fatty acids.[45] *Cpt1a* and *Cpt1b* were not altered with the treatment of TGFb1 for 2 days(Figure 5G), although *Cpt1a* displayed downregulation along trajectory (Figure XIV in the online-only Data Supplement). Moreover, *Crat* level was significantly downregulated first and then upregulated during SMC differentiation, which is supported by the early downregulation and late upregulation of *Crat* level along SMC trajectory (Figure 5I and Figure XIV in the online-only Data Supplement). Thus, significant metabolic reprogramming was induced during SMC differentiation, and altered lipid metabolism implied the involvement of *Crat* in SMC differentiation.

TGFb1 Promotes SMC Differentiation via Inhibition of Crat

In SMC differentiation, TGFb1 altered the lipid profile and inhibited the level of Crat. To confirm the role of *Crat in* SMC differentiation, siRNA *Crat* was utilized. Q-PCR showed successful knockdown of *Crat* 2 days after *Crat* siRNA transfection (Figure 6A). SMC markers including *Cnn1, Tagln* and *Acta2* were induced at the mRNA level (Figure 6A) by *Crat* siRNA transfection. Promotion of SMC differentiation by *Crat* knockdown was demonstrated at the protein level by Western blot (Figure 6B) and immunofluorescent staining (Figure 6C) 2 days after *Crat* siRNA transfection. The upregulation of TGFb1 at the mRNA level (Figure 6D) and the protein level (Figure 6E and 6F) 2 days after *Crat* siRNA transfection identified the induction of TGFb1 as the downstream mechanism of Crat-

mediated SMC differentiation. To conclude, an interesting feedback control was identified between Crat inhibition and TGFb1 induction during differentiation.

MiR-378a-3p Induces Metabolic Reprogramming and Promotes SMC Differentiation

After establishing the change of the metabolic profile during differentiation process and the mechanism involved in SMC differentiation, potential therapeutic targets that could similarly alter the metabolic profile and drive SMC differentiation were investigated. Literature mining revealed that miR-378a-3p could target *Crat* and thus regulate fatty acid metabolism which was regulated by TGFb1 in our SMC differentiation system.[46] To study the role of miR-378a-3p in metabolic reprogramming and SMC differentiation, PV-ADSCs were transfected with miR-378a-3p mimics. In Seahorse Mito Stress tests, both the basal OCR and maximal OCR showed an increasing trend with miR-378a-3p mimic treatment compared with control (Figure 7A). Furthermore, the mitochondrial potential also increased (Figure 7B). Metabolite abundance detected by GC-MS system demonstrated the enrichment of metabolites involved in the TCA cycle (Figure 7C) and upregulated level of various lipids such as cholesterol (Figure 7D). Overall, the metabolic reprogramming induced by the miR-378a-3p mimics was similar to that induced by TGFb1. Furthermore, miR-378a-3p mimics induced SMC differentiation with the significant upregulation of *Cnn1* and *Tagln* (Figure 7E). The induction of SMC gene expression was confirmed at the protein level (Figure 7F and Figure XVA in the online-only Data Supplement). On the contrary, miR-378a-3p inhibitor downregulated mRNA level of SMC markers (Figure 7G). In addition, Crat expression was also de-repressed in PV-ADSCs after the transfection of miR-378a-3p inhibitors (Figure 7G).

Finally, TGFb1 treatment could not induce an upregulation of OCR and ECAR in ADSCs derived from miR-378a-3p knock out mice (Figure 7H), further confirming the importance of miR-378a in inducing metabolic reprogramming. Also, SMC differentiation capacity was significantly attenuated in ADSCs derived from miR-378a knockout mice as shown by the lower level of CNN1 compared with ADSCs from wild type mice after the treatment with TGFb1 (Figure 7I and Figure XVB in the online-only Data Supplement). Interestingly, level of miR-378a-3p was downregulated by TGFb1 treatment (Figure XVC in the online-only Data Supplement). In summary, metabolic reprogramming and SMC differentiation were induced by miR-378a-3p, which was an indispensable component for TGFb1 to exert the metabolic regulation.

Discussion

In this study, we characterized the transcriptomic profile of PV-ADSCs at a single-cell level and determined their role in vascular remodeling through their differentiation towards smooth muscle lineage which was accompanied by metabolic reprogramming. Substantial heterogeneity was observed at the single-cell level in primary PV-ADSCs. Moreover, through differentiation towards smooth muscle lineage, cultured PV-ADSCs were suggested to contribute to vascular remodeling in vein graft models. Mechanistically, SMC differentiation from PV-ADSCs was accompanied by a metabolic reprogramming which could be induced by miR-378a-3p.

To characterize the PV-ADSCs, scRNA-seq was performed and revealed two distinct clusters within the $CD45^-/CDH5^-/CD29^+/Sca1^+$ population, as well as the signature gene sets and feature signaling pathways for each cluster. However, attention needs to be paid to the markers used to identify the MSCs. About 60.15% ± 3.77% of the $CD45^-/CDH5^-$ population were $CD29^+/Sca1^+$. Thus, the scRNA-seq result only covers this population and remaining cells necessitate further characterization. Furthermore, multiple cluster 1 markers including *Pecam1* and *Cd36* displayed low percentage expression in *in vitro* cultured PV-ADSCs, which suggested difficult retainment of these markers in present culture condition or selective expansion of cluster 2 cells. Future efforts including selective culture of cells from each cluster and separate determination of their contribution to vascular remodeling are needed.

Consistent with what has been reported for MSCs[47, 48], considerable heterogeneity of PV-ADSCs has been observed in our study, which serves as direct evidence for stem cells from the perivascular

(peri-aorta) adipose tissue. Although transcriptional network heterogeneity of stromal vascular fraction from axillary adipose tissue was reported[49], perivascular adipose tissue is more relevant to vascular function.[1] With scRNA-seq, heterogeneous intracellular markers and functional modules have also been described in our study. Due to this substantial heterogeneity, markers that are used to identify MSC population by itself, such as *Tbx18*[37], might only label a sub-population. To overcome the laborious efforts to generate lineage tracing models for all the heterogeneously expressed markers utilized for MSC identification, more specific markers need to be discovered. In our study, *Tgfbr2* and *Anxa1* characterize cluster 2 PV-ADSCs specifically and bears the potential to identify this population homogenously *in vivo*. However, because of the limited number of primary PV-ADSCs, only a small number of cells were sequenced in our study. This is one limitation of the study. Sequencing of more primary cells would provide the possibility to discover better identity markers unique for MSC population or sub-population. Another limitation of the study mainly lies in the lack of *in vivo* evidence for PV-ADSC contribution to vascular injury repair. Future investigation of *in vivo* PV-ADSC fate labeled by markers found by this study and future scRNA-seq data with larger cell number are needed.

Under disease settings such as atherosclerosis and vascular injury, adventitia stem cells migrate to the injury site and differentiate towards vascular lineages in response to the cytokine profile changes.[50, 51] Similar explorations of PV-ADSC responses in diseased status would provide novel therapeutic insights. Cell transplantation experiments of RFP-labeled PV-ADSCs in vein graft transplantation experiments confirmed their involvement in vascular remodeling, similar to adventitia stem cells. Preliminary result demonstrating the migration of PV-ADSCs towards chemoattractant SDF-1 suggests that cell migration is among the complex mechanisms through which PV-ADSCs participate in vascular injury repair, and thus is a potentially interesting field. These findings together expand the pool of the resident vascular stem cell population consisting adventitia stem cells to include MSCs that reside in the PVAT. Lineage tracing studies with markers identified by scRNA-seq are in need to further assess the *in vivo* physiological and pathophysiological role of PV-ADSCs.

Regarding the differentiation mechanism, accumulating evidence has demonstrated the importance of metabolic reprogramming in stem cell differentiation.[11, 44] It was shown that increased glycolysis is associated with pluripotency and increased mitochondrial respiration is associated with differentiation in pluripotent stem cells.[52] MSCs displayed suppressed glycolysis when driven to differentiation towards osteocytes.[53] Our study characterized the metabolic profile change of PV-ADSCs during SMC differentiation and proposed the importance of lipid metabolism in regulating the differentiation process. MiR-378-3a bears potential in regulating SMC differentiation. Efforts are needed to further validate the function of miR-378-3a in vascular injury models and explore its therapeutic potential.

Evidence of the important role of the adipose-vascular crosstalk in various metabolic diseases has identified novel targets such as perivascular relaxing factors[54] or secreted adipokines[55] with significant therapeutic potential. By demonstrating the role of PV-ADSCs in vascular remodeling through metabolism-related regulation of SMC differentiation, our results support the need to further investigate the role of PV-ADSCs in vascular remodeling in various metabolic diseases such as atherosclerosis and diabetes mellitus. The process of PV-ADSC-involved vascular remodeling, which was not recognized before, might be targeted in future therapeutic development for metabolic diseases. Potential future exploration also includes the influence of adipokines secreted by perivascular adipose tissue on PV-ADSC differentiation and function, especially under disease conditions, given that preliminary results have shown the promoting effect of IGFBP-2 on SMC differentiation. Collectively, our study provides direct evidence of PV-ADSC heterogeneity through high-resolution characterization with scRNA-seq and suggests their participation in vascular remodeling through SMC differentiation driven by metabolic reprogramming which necessitate confirmation with further *in vivo* lineage tracing experiments. Taken together, the results imply the previously unappreciated identity and function of PV-ADSCs in vascular remodeling, unveil the mechanism for SMC differentiation from a metabolic perspective and provide insights for future studies to investigate the role of PV-ADSCs in various metabolic diseases.

Acknowledgments

The authors acknowledge financial support from the Department of Health via the National Institute for Health Research (NIHR) comprehensive Biomedical Research Centre award to Guy's & St Thomas' NHS Foundation Trust in partnership with King's College London and King's College Hospital NHS Foundation Trust. NMR experiments were produced using the facilities of the Centre for Biomolecular Spectroscopy, King's College London, acquired with a Multi-user Equipment Grant from the Wellcome Trust and an Infrastructure Grant from the British Heart Foundation. Breeding of miR-378a knockout mice was supported by the MAESTRO and OPUS grants of the Polish National Science Center [2012/06/A/NZ1/0004, 2012/07/B/NZ1/02881] to J.Du.

Sources of Funding

This work is supported by the British Heart Foundation (RG/14/6/31144).

Disclosures

None.

References

1. Rajsheker S, Manka D, Blomkalns AL, Chatterjee TK, Stoll LL, Weintraub NL. Crosstalk between perivascular adipose tissue and blood vessels. *Curr Opin Pharmacol*. 2010;10:191-196.
2. Omar A, Chatterjee TK, Tang Y, Hui DY, Weintraub NL. Proinflammatory phenotype of perivascular adipocytes. *Arterioscler Thromb Vasc Biol*. 2014;34:1631-1636.
3. Chang L, Villacorta L, Li R, Hamblin M, Xu W, Dou C, Zhang J, Wu J, Zeng R, Chen YE. Loss of perivascular adipose tissue on peroxisome proliferator-activated receptor-gamma deletion in smooth muscle cells impairs intravascular thermoregulation and enhances atherosclerosis. *Circulation*. 2012;126:1067-1078.
4. Manka D, Chatterjee TK, Stoll LL, Basford JE, Konaniah ES, Srinivasan R, Bogdanov VY, Tang Y, Blomkalns AL, Hui DY, Weintraub NL. Transplanted perivascular adipose tissue accelerates injury-induced neointimal hyperplasia: Role of monocyte chemoattractant protein-1. *Arterioscler Thromb Vasc Biol*. 2014;34:1723-1730.
5. Barker N, Bartfeld S, Clevers H. Tissue-resident adult stem cell populations of rapidly self-renewing organs. *Cell Stem Cell*. 2010;7:656-670.
6. Hu Y, Zhang Z, Torsney E, Afzal AR, Davison F, Metzler B, Xu Q. Abundant progenitor cells in the adventitia contribute to atherosclerosis of vein grafts in apoe-deficient mice. *J Clin Invest*. 2004;113:1258-1265.
7. Zhang L, Issa Bhaloo S, Chen T, Zhou B, Xu Q. Role of resident stem cells in vessel formation and arteriosclerosis. *Circ Res*. 2018;122:1608-1624.
8. Lin G, Garcia M, Ning H, Banie L, Guo YL, Lue TF, Lin CS. Defining stem and progenitor cells within adipose tissue. *Stem Cells Dev*. 2008;17:1053-1063.
9. Fraser JK, Schreiber R, Strem B, Zhu M, Alfonso Z, Wulur I, Hedrick MH. Plasticity of human adipose stem cells toward endothelial cells and cardiomyocytes. *Nat Clin Pract Cardiovasc Med*. 2006;3 Suppl 1:S33-37.
10. Wilson NK, Kent DG, Buettner F, et al. Combined single-cell functional and gene expression analysis resolves heterogeneity within stem cell populations. *Cell Stem Cell*. 2015;16:712-724.
11. Gu W, Gaeta X, Sahakyan A, Chan AB, Hong CS, Kim R, Braas D, Plath K, Lowry WE, Christofk HR. Glycolytic metabolism plays a functional role in regulating human pluripotent stem cell state. *Cell Stem Cell*. 2016;19:476-490.

12. Ito K, Carracedo A, Weiss D, Arai F, Ala U, Avigan DE, Schafer ZT, Evans RM, Suda T, Lee CH, Pandolfi PP. A pml-ppar-delta pathway for fatty acid oxidation regulates hematopoietic stem cell maintenance. *Nat Med*. 2012;18:1350-1358.
13. Pertea M, Kim D, Pertea GM, Leek JT, Salzberg SL. Transcript-level expression analysis of rna-seq experiments with hisat, stringtie and ballgown. *Nat Protoc*. 2016;11:1650-1667.
14. Buettner F, Natarajan KN, Casale FP, Proserpio V, Scialdone A, Theis FJ, Teichmann SA, Marioni JC, Stegle O. Computational analysis of cell-to-cell heterogeneity in single-cell rna-sequencing data reveals hidden subpopulations of cells. *Nat Biotechnol*. 2015;33:155-160.
15. Gardeux V, David FPA, Shajkofci A, Schwalie PC, Deplancke B. Asap: A web-based platform for the analysis and interactive visualization of single-cell rna-seq data. *Bioinformatics*. 2017;33:3123-3125.
16. Dennis G, Jr., Sherman BT, Hosack DA, Yang J, Gao W, Lane HC, Lempicki RA. David: Database for annotation, visualization, and integrated discovery. *Genome Biol*. 2003;4:P3.
17. Subramanian A, Tamayo P, Mootha VK, Mukherjee S, Ebert BL, Gillette MA, Paulovich A, Pomeroy SL, Golub TR, Lander ES, Mesirov JP. Gene set enrichment analysis: A knowledge-based approach for interpreting genome-wide expression profiles. *Proc Natl Acad Sci U S A*. 2005;102:15545-15550.
18. Butler A, Hoffman P, Smibert P, Papalexi E, Satija R. Integrating single-cell transcriptomic data across different conditions, technologies, and species. *Nat Biotechnol*. 2018;36:411-420.
19. Merrick D, Sakers A, Irgebay Z, Okada C, Calvert C, Morley MP, Percec I, Seale P. Identification of a mesenchymal progenitor cell hierarchy in adipose tissue. *Science*. 2019;364
20. Schwalie PC, Dong H, Zachara M, Russeil J, Alpern D, Akchiche N, Caprara C, Sun W, Schlaudraff KU, Soldati G, Wolfrum C, Deplancke B. A stromal cell population that inhibits adipogenesis in mammalian fat depots. *Nature*. 2018;559:103-108.
21. Trapnell C, Cacchiarelli D, Grimsby J, Pokharel P, Li S, Morse M, Lennon NJ, Livak KJ, Mikkelsen TS, Rinn JL. The dynamics and regulators of cell fate decisions are revealed by pseudotemporal ordering of single cells. *Nat Biotechnol*. 2014;32:381-386.
22. Kanamori M, Konno H, Osato N, Kawai J, Hayashizaki Y, Suzuki H. A genome-wide and nonredundant mouse transcription factor database. *Biochem Biophys Res Commun*. 2004;322:787-793.
23. Beronja S, Livshits G, Williams S, Fuchs E. Rapid functional dissection of genetic networks via tissue-specific transduction and rnai in mouse embryos. *Nat Med*. 2010;16:821-827.
24. Le Bras A, Yu B, Issa Bhaloo S, Hong X, Zhang Z, Hu Y, Xu Q. Adventitial sca1+ cells transduced with etv2 are committed to the endothelial fate and improve vascular remodeling after injury. *Arterioscler Thromb Vasc Biol*. 2018;38:232-244.
25. Gu W, Hong X, Le Bras A, Nowak WN, Issa Bhaloo S, Deng J, Xie Y, Hu Y, Ruan XZ, Xu Q. Smooth muscle cells differentiated from mesenchymal stem cells are regulated by micrornas and suitable for vascular tissue grafts. *J Biol Chem*. 2018;293:8089-8102.
26. Xu Q, Zhang Z, Davison F, Hu Y. Circulating progenitor cells regenerate endothelium of vein graft atherosclerosis, which is diminished in apoe-deficient mice. *Circ Res*. 2003;93:e76-86.
27. Kozlowska J, Rivett DW, Vermeer LS, Carroll MP, Bruce KD, Mason AJ, Rogers GB. A relationship between pseudomonal growth behaviour and cystic fibrosis patient lung function identified in a metabolomic investigation. *Metabolomics*. 2013;9
28. Sellick CA, Croxford AS, Maqsood AR, Stephens G, Westerhoff HV, Goodacre R, Dickson AJ. Metabolite profiling of recombinant cho cells: Designing tailored feeding regimes that enhance recombinant antibody production. *Biotechnol Bioeng*. 2011;108:3025-3031.
29. Worley B, Powers R. Multivariate analysis in metabolomics. *Curr Metabolomics*. 2013;1:92-107.
30. Xia J, Sinelnikov IV, Han B, Wishart DS. Metaboanalyst 3.0--making metabolomics more meaningful. *Nucleic Acids Res*. 2015;43:W251-257.

31. Crisan M, Yap S, Casteilla L, et al. A perivascular origin for mesenchymal stem cells in multiple human organs. *Cell Stem Cell*. 2008;3:301-313.
32. Tabatabaei Qomi R, Sheykhhasan M. Adipose-derived stromal cell in regenerative medicine: A review. *World J Stem Cells*. 2017;9:107-117.
33. Stzepourginski I, Nigro G, Jacob JM, Dulauroy S, Sansonetti PJ, Eberl G, Peduto L. Cd34+ mesenchymal cells are a major component of the intestinal stem cells niche at homeostasis and after injury. *Proc Natl Acad Sci U S A*. 2017;114:E506-E513.
34. Horwitz EM, Le Blanc K, Dominici M, Mueller I, Slaper-Cortenbach I, Marini FC, Deans RJ, Krause DS, Keating A, International Society for Cellular T. Clarification of the nomenclature for msc: The international society for cellular therapy position statement. *Cytotherapy*. 2005;7:393-395.
35. Chen Y, Wong MM, Campagnolo P, Simpson R, Winkler B, Margariti A, Hu Y, Xu Q. Adventitial stem cells in vein grafts display multilineage potential that contributes to neointimal formation. *Arterioscler Thromb Vasc Biol*. 2013;33:1844-1851.
36. Houlihan DD, Mabuchi Y, Morikawa S, Niibe K, Araki D, Suzuki S, Okano H, Matsuzaki Y. Isolation of mouse mesenchymal stem cells on the basis of expression of sca-1 and pdgfr-alpha. *Nat Protoc*. 2012;7:2103-2111.
37. Guimaraes-Camboa N, Cattaneo P, Sun Y, Moore-Morris T, Gu Y, Dalton ND, Rockenstein E, Masliah E, Peterson KL, Stallcup WB, Chen J, Evans SM. Pericytes of multiple organs do not behave as mesenchymal stem cells in vivo. *Cell Stem Cell*. 2017;20:345-359 e345.
38. Takahashi K, Yamanaka S. Induction of pluripotent stem cells from mouse embryonic and adult fibroblast cultures by defined factors. *Cell*. 2006;126:663-676.
39. Merkel M, Eckel RH, Goldberg IJ. Lipoprotein lipase: Genetics, lipid uptake, and regulation. *J Lipid Res*. 2002;43:1997-2006.
40. Ji C, Liu X, Xu L, Yu T, Dong C, Luo J. Runx1 plays an important role in mediating bmp9-induced osteogenic differentiation of mesenchymal stem cells line c3h10t1/2, murine multi-lineage cells lines c2c12 and mefs. *Int J Mol Sci*. 2017;18
41. Wang Y, Chen X, Cao W, Shi Y. Plasticity of mesenchymal stem cells in immunomodulation: Pathological and therapeutic implications. *Nat Immunol*. 2014;15:1009-1016.
42. Gu W, Ni Z, Tan YQ, Deng J, Zhang SJ, Lv ZC, Wang XJ, Chen T, Zhang Z, Hu Y, Jing ZC, Xu Q. Adventitial cell atlas of wt (wild type) and apoe (apolipoprotein e)-deficient mice defined by single-cell rna sequencing. *Arterioscler Thromb Vasc Biol*. 2019;39:1055-1071.
43. Villarroya F, Cereijo R, Villarroya J, Giralt M. Brown adipose tissue as a secretory organ. *Nat Rev Endocrinol*. 2017;13:26-35.
44. Chandel NS, Jasper H, Ho TT, Passegue E. Metabolic regulation of stem cell function in tissue homeostasis and organismal ageing. *Nat Cell Biol*. 2016;18:823-832.
45. Goldberg EL, Dixit VD. Carnitine acetyltransferase (crat) expression in macrophages is dispensable for nutrient stress sensing and inflammation. *Mol Metab*. 2017;6:219-225.
46. Krist B, Florczyk U, Pietraszek-Gremplewicz K, Jozkowicz A, Dulak J. The role of mir-378a in metabolism, angiogenesis, and muscle biology. *Int J Endocrinol*. 2015;2015:281756.
47. Pevsner-Fischer M, Levin S, Zipori D. The origins of mesenchymal stromal cell heterogeneity. *Stem Cell Rev*. 2011;7:560-568.
48. Gu W, Hong X, Potter C, Qu A, Xu Q. Mesenchymal stem cells and vascular regeneration. *Microcirculation*. 2017;24
49. Hardy WR, Moldovan NI, Moldovan L, Livak KJ, Datta K, Goswami C, Corselli M, Traktuev DO, Murray IR, Peault B, March K. Transcriptional networks in single perivascular cells sorted from human adipose tissue reveal a hierarchy of mesenchymal stem cells. *Stem Cells*. 2017;35:1273-1289.
50. Xie Y, Potter CMF, Le Bras A, Nowak WN, Gu W, Bhaloo SI, Zhang Z, Hu Y, Zhang L, Xu Q. Leptin induces sca-1(+) progenitor cell migration enhancing neointimal lesions in vessel-injury mouse models. *Arterioscler Thromb Vasc Biol*. 2017;37:2114-2127.

51. Yu B, Kiechl S, Qi D, et al. A cytokine-like protein dickkopf-related protein 3 is atheroprotective. *Circulation*. 2017;136:1022-1036.
52. Xu X, Duan S, Yi F, Ocampo A, Liu GH, Izpisua Belmonte JC. Mitochondrial regulation in pluripotent stem cells. *Cell Metab*. 2013;18:325-332.
53. Daud H, Browne S, Al-Majmaie R, Murphy W, Al-Rubeai M. Metabolic profiling of hematopoietic stem and progenitor cells during proliferation and differentiation into red blood cells. *N Biotechnol*. 2016;33:179-186.
54. Gollasch M. Adipose-vascular coupling and potential therapeutics. *Annu Rev Pharmacol Toxicol*. 2017;57:417-436.
55. Akoumianakis I, Tarun A, Antoniades C. Perivascular adipose tissue as a regulator of vascular disease pathogenesis: Identifying novel therapeutic targets. *Br J Pharmacol*. 2017;174:3411-3424.

Highlights

- Single-cell RNA sequencing allows direct visualization of PV-ADSC heterogeneity at a single-cell level and uncovers two sub-populations with distinct signature genes and signaling pathways.
- The function of PVAT in vascular regeneration are partly attributed to PV-ADSCs and their differentiation towards smooth muscle lineage.
- TGFb1 and miR-378a-3p mimics induced a similar metabolic reprogramming of PV-ADSCs, including upregulated mitochondrial potential and altered lipid levels such as increased cholesterol and promoted smooth muscle differentiation.

Figure Legends

Figure 1. Characterization of PV-ADSCs. A and **B**, Representative histograms of flow cytometry analysis of cultured PV-ADSCs and the percentage of indicated phenotypic markers (n=3). Gating is set for the IgG control to be between 0.5% to 1%. **C**, Immunofluorescent staining of the adipose tissue surrounding the mouse aorta with CD29, Sca1, PECAM1, PLIN1 and DAPI (n=3). Arrows indicate the $CD29^{+}$/$Sca1^{+}$/$PECAM1^{-}$/$PLIN1^{-}$ cells. The border between End (endothelium), Med (media), Adv (adventitia) and PVAT (perivascular adipose tissue) is drawn with dashed line. Scale bar, 50 μm. Ctrl indicates IgG isotype control; DAPI, 4′,6-diamidino-2-phenylindole; and PV-ADSCs, perivascular adipose tissue-derived mesenchymal stem cells.

Figure 2. ScRNA-seq reveals two distinct clusters in PV-ADSCs. A, Sorting gate for scRNA-seq was set as live nucleated cells ($Syto16^{+}$/$DAPI^{-}$), single cells, $CD45^{-}$/$CDH5^{-}$ cells and $CD29^{+}$/$Sca1^{+}$ cells. **B**, Scatter plot obtained from MDS analysis showed two distinct clusters. Color scale, log2(gene counts). **C**, Expression of representative genes for cluster 1 (*Cd36*) and cluster 2 (*Tgfbr2*). **D**, Heatmap of marker genes in each cluster. Color scale, log2(gene counts). Full list of genes was in Table I in the online-only Data Supplement. **E** and **F**, Gene ontology and KEGG pathway analysis of the top 200 genes (by *P* value) upregulated in Cluster 1 (**E**) and Cluster 2 (**F**). Full list of GO terms and KEGG pathways was in Table II in the online-only Data Supplement. **G**, Enrichment of gene sets including Myogenesis (Molecular Signature) and TGF-b signaling (KEGG). **H**, Expression heatmap of frequently-used MSC markers. Color scale, log2(gene counts). **I**, Expression of frequently-used MSC markers in the two clusters was shown as violin plot. Cl 1 indicates cluster 1; Cl 2, cluster 2; FDR, false discovery rate; GOMF, gene ontology molecular function; KEGG, Kyoto encyclopedia of genes and genomes; and NES, normalized enrichment score.

Figure 3. Pseudotime trajectory of cultured PV-ADSCs. A, Cell stages expressing early to late SMC markers. **B**, Pseudotime trajectory of cultured PV-ADSCs with "DDRTree" method for dimension reduction. Color scale, pseudotime. **C**, Cell ordering from different differentiation stages along the pseudotime trajectory. **D**, Heatmap of the top 1000 (by q value) significantly changed genes in three gene modules. **E**, Expression of *Ly6a*, *Cnn1* and *Myh11* along the trajectory. Color scale, log

gene expression. **F**, Gene ontology (molecular function) analysis of each gene module from (**D**). Full list was in Table III in the online-only Data Supplement. **G**, Expression of significantly changed genes from TGF-b signaling pathway (KEGG) along pseudotime. Full list was in Table I in the online-only Data Supplement. Color scale, log gene expression. **H**, *Tgfb2* expression and total level of significantly changed genes from TGF-b signaling along the pseudotime trajectory. Color scale, log gene expression. **I**, Expression of significantly changed transcription factors along the pseudotime trajectory. Full list was in Table I in the online-only Data Supplement. Color scale, log gene expression.

Figure 4. PV-ADSCs differentiate towards SMCs *in vivo* and *in vitro*. **A**, H&E staining of the vein graft harvested 4 weeks after the transplantation. Neointimal area was calculated against injury-only control (n=4). Arrow indicates the boundary between neo-intima and media layer. **B**, Vein grafts harvested one week after the transplantation were stained with RFP (red) and SMC marker ACTA2 (green) (n=4). Arrows indicate cells positive for both markers. Dashed line indicates boundary of adventitia and neointima. Scale bar, 20 μm. **C-E**, *In vitro* cultured PV-ADSCs were differentiated towards SMCs in differentiation medium for 5 days (diff) and then harvested for Q-PCR (**C**) (n=4), Western blot (**D**) (n=3) and immunofluorescent staining (**E**) (n=3) for SMC markers. Cells cultured without TGFb1 (ctrl) served as control. Scale bar, 20 μm. **F**, Chemotaxis of PV-ADSCs in response to an increasing gradient of SDF1 in an 8.0-μm transwell system was identified by applying 1% crystal violet staining after 16-h incubation (n=3). Scale bar, 50 μm. **G**, H&E staining of subcutaneous *Matrigel* plug containing PV-ADSCs-derived SMCs and ECs (diff) in comparison with control group (ctrl) (n=4). **H**, Immunostaining of the tube-like structure in *Matrigel* plug with ACTA2 and PECAM1 (n=4). Scale bar, 50 μm. Data are presented as mean±SD. **P*<0.05, ***P*<0.01. Adv indicates adventitia.

Figure 5. Metabolic reprogramming of PV-ADSCs during SMC differentiation. **A** and **B**, Cellular metabolite abundance was detected with NMR system in undifferentiated PV-ADSCs and PV-ADSCs differentiated for 1 day (n=8). **A**, Heatmap for metabolite levels. **B**, Orthogonal projection to latent structures. **C,** The OCR measured in PV-ADSCs cultured with or without TGFb1 for 1 day (n=3). **D**, Live PV-ADSCs cultured in differentiation medium or basal growth medium for 1 day and 4 days were stained TMRM to detect mitochondrial potential (n=3). **E** and **F**, Cellular metabolite abundance in undifferentiated PV-ADSCs or PV-ADSCs differentiated for 4 days was determined with GC-MS system (n=3). Heatmaps of metabolites involved in TCA cycle (**E**) or lipid metabolism (**F**) were shown. **G**, Gene expression of genes important in lipid metabolism in PV-ADSCs treated with or without TGFb1 for 2 days (n=4). **H**, Expression of *Cebpb* along the pseudotime trajectory. Color scale, log expression of gene. **I**, *Crat* mRNA level in PV-ADSCs treated with or without TGFb1 for 2 days (n=4). Data are presented as mean±SD. **P*<0.05, ***P*<0.01 and ****P*<0.001. Anti-A/Rot indicates anti-mycin A/Rotenone; FCCP, carbonyl cyanide-4-phenylhydrazone; MFI, mean fluorescence intensity; OCR, oxygen consumption rate; Oligo, oligomycin; SRC, spare respiratory consumption; and TMRM, Tetramethylrhodamine, Methyl Ester, Perchlorate.

Figure 6. *Crat* knockdown promotes SMC differentiation via upregulation of TGFb1. A-C, PV-ADSCs treated with Crat siRNA with or without TGFb1 for two days. **A**, *Crat* level was significantly downregulated after siRNA Crat transfection. Q-PCR also showed the induction of SMC markers (*Cnn1, Tagln* and *Acta2*) with Crat knockdown. **B**, Protein level induction of SMC markers by Crat siRNA was demonstrated by Western blot**. C**, Immunostaining and statistical analysis showed the induction of SMC markers by Crat siRNA in medium without TGFb1. **D-F**, TGFb1 level after Crat siRNA transfection for 2 days was determined with Q-PCR (**D**), Western blot (**E**) and immunofluorescent staining (**F**). Results are cumulative (A and D) or representative (B, C, E and F) of three independent experiments. Scale bar, 30 μm. Data are presented as mean±SD. **P*<0.05, ***P*<0.01 and ****P*<0.001.

Figure 7. miR-378a-3p induces metabolic reprogramming and promotes SMC differentiation. A, The OCR of PV-ADSCs cultured in miR-378a-3p mimics or control for 2 days (n=3). **B**, Live PV-ADSCs treated with miR-378a-3p mimic for 2 days with or without TGFb1 were stained TMRM and analyzed for MFI with flow cytometry (n=3). **C** and **D**, Cellular metabolite abundance in PV-ADSCs treated with miR-378a-3p mimics for 1 day determined with GC-MS system (n=3). Heatmap of

metabolites in TCA cycle (**C**) or lipid metabolism (**D**). **E**, SMC marker mRNAs were induced by miR-378a-3p mimics after 2 days (n=3). **F**, Representative immunofluorescent staining (n=3) showed the upregulation of SMC markers by miR-378a-3p mimic treatment. **G**, Transfection of PV-ADSCs with miR-378a-3p inhibitor inhibited the level of SMC markers as shown by Q-PCR. The level of *Crat* was de-repressed by miR-378a-3p inhibitor transfection (n=3). **H**, OCR and ECAR were detected with Seahorse Mito stress tests in wild-type (WT) and miR-378a knockout (KO) ADSCs (n=3). **I**, Wild-type (WT) and miR-378a knockout (KO) ADSCs were treated with or without TGFb1 for 2 days. Immunofluorescent staining showed the protein level of CNN1 (n=1). Scale bar, 100 μm. Data are mean±SD. **P*<0.05 and ***P*<0.01. Anti-A/Rot indicates anti-mycin A/Rotenone; Crat, carnitine acetyltransferase; FCCP, carbonyl cyanide-4-phenylhydrazone; inh 378, miR-378a-3p inhibitor; inh ctrl, inhibitor control; MFI, mean fluorescence intensity; mim 378, miR-378a-3p mimics; mim ctrl, mimics control; OCR, oxygen consumption rate; oligo, oligomycin; SRC, spare respiratory capacity; and TMRM, Tetramethylrhodamine, Methyl Ester, Perchlorate.

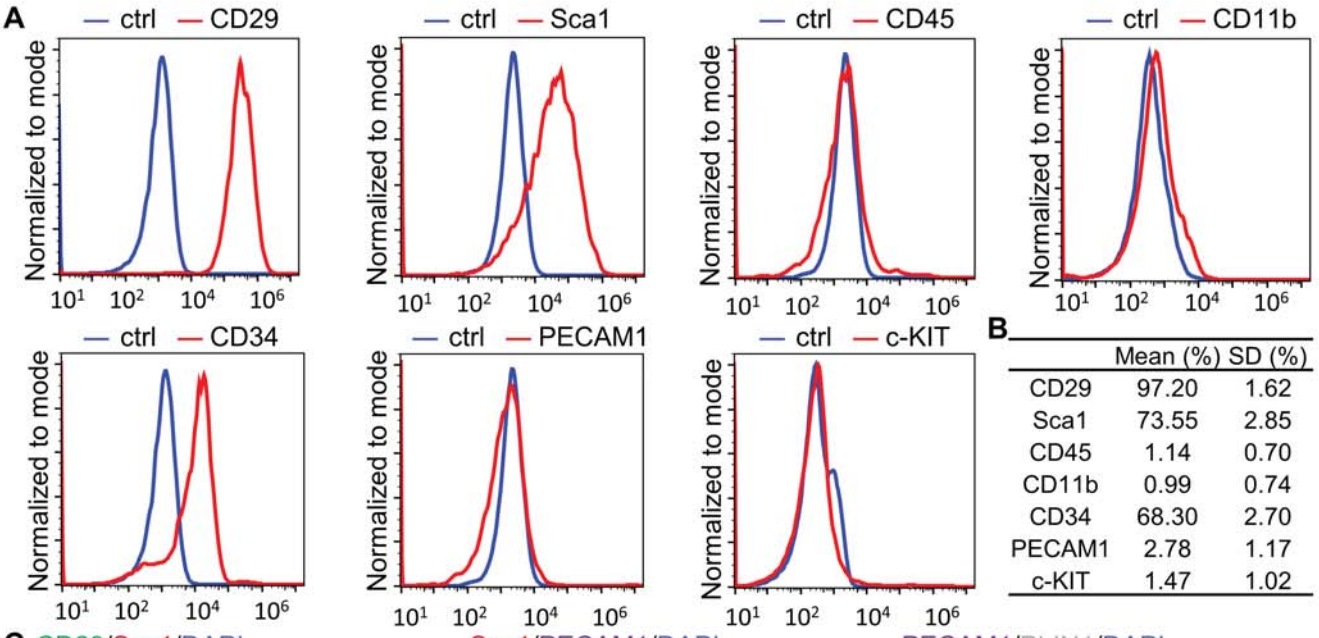

B

	Mean (%)	SD (%)
CD29	97.20	1.62
Sca1	73.55	2.85
CD45	1.14	0.70
CD11b	0.99	0.74
CD34	68.30	2.70
PECAM1	2.78	1.17
c-KIT	1.47	1.02

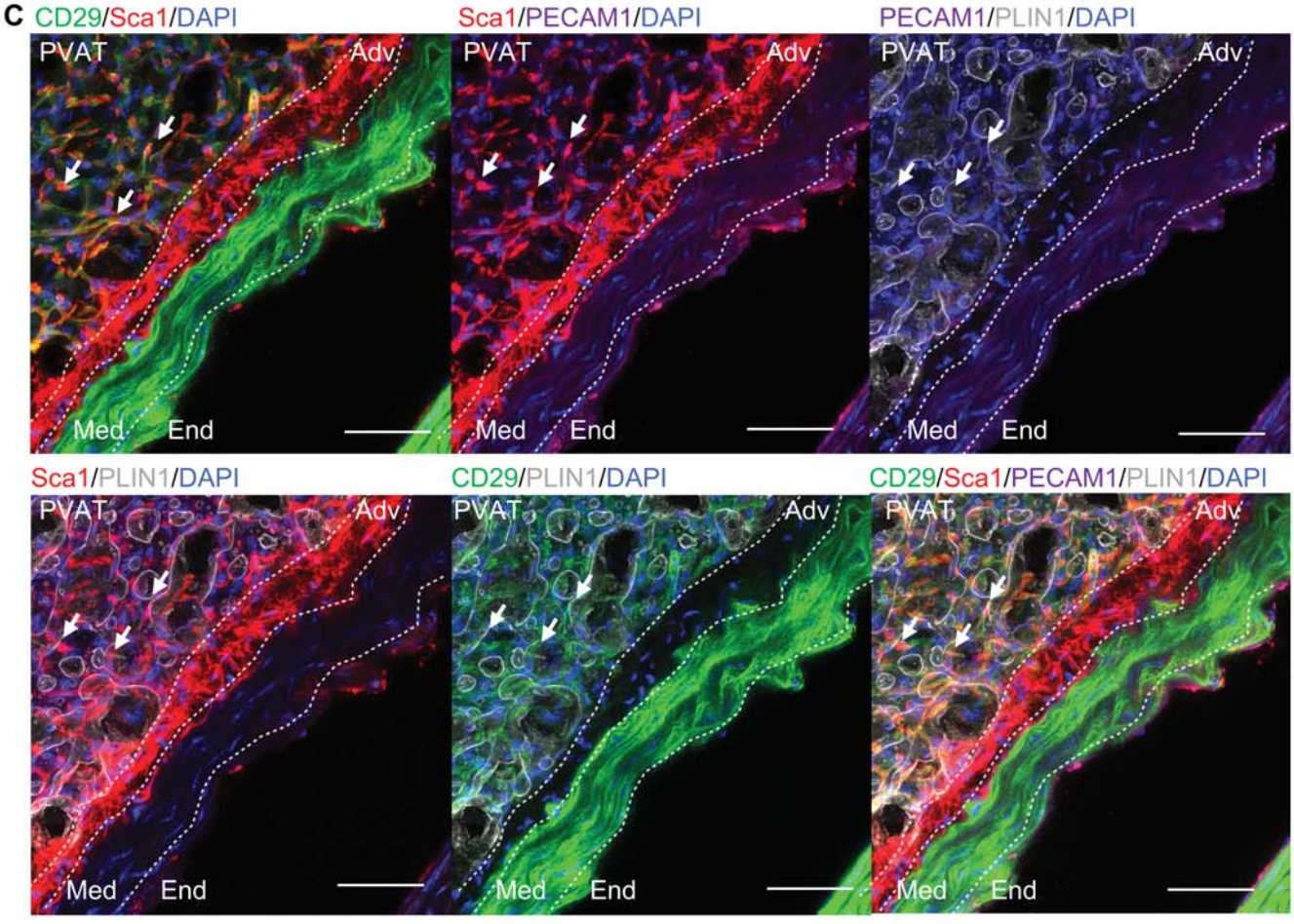

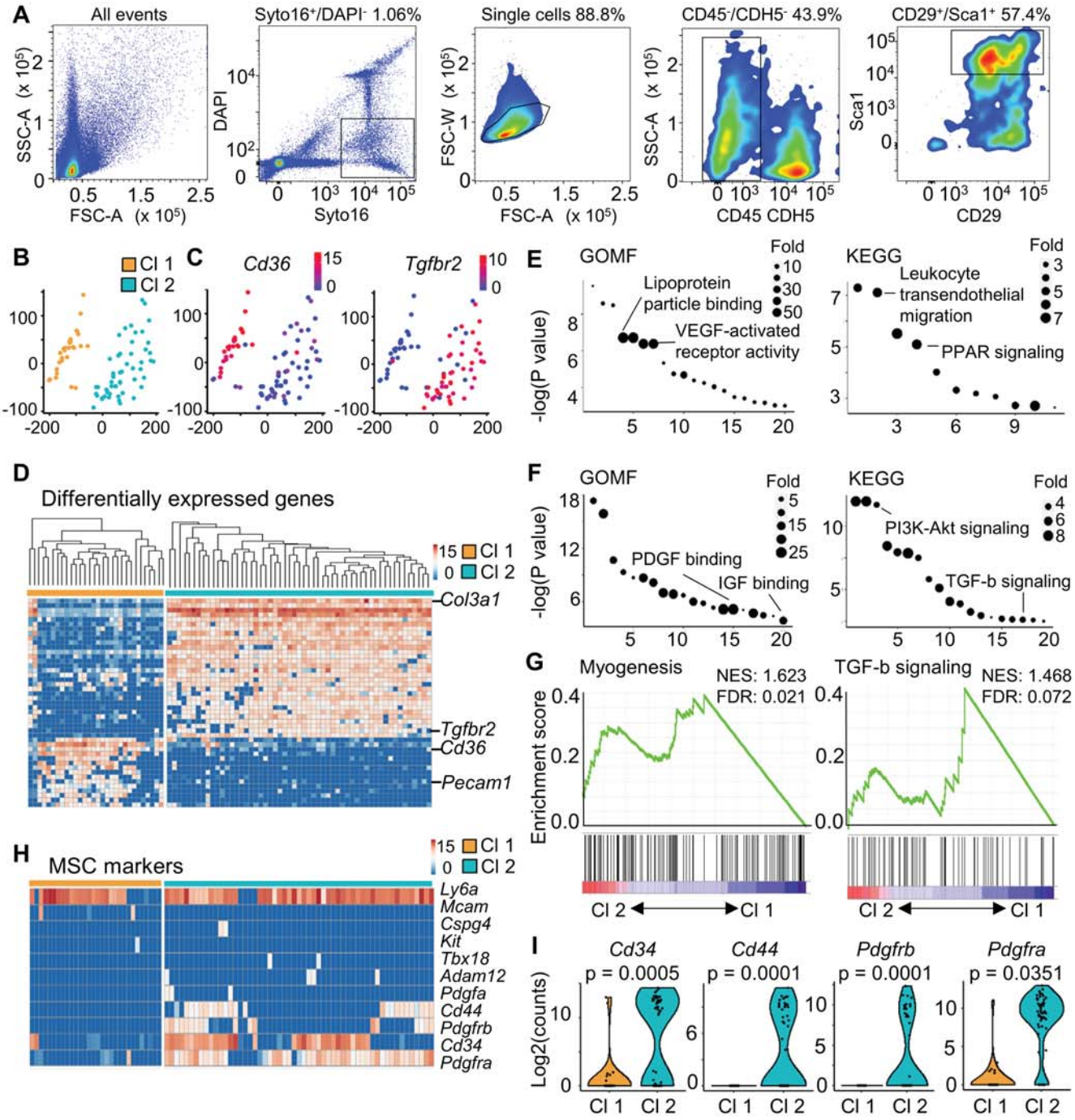
A
All events
Syto16+/DAPI- 1.06%
Single cells 88.8%
CD45-/CDH5- 43.9%
CD29+/Sca1+ 57.4%
SSC-A (x 10^5)
FSC-A (x 10^5)
DAPI
Syto16
FSC-W (x 10^5)
CD45 CDH5
Sca1
CD29
B
Cl 1
Cl 2
C
Cd36
Tgfbr2
D
Differentially expressed genes
Col3a1
Tgfbr2
Cd36
Pecam1
E
GOMF
Lipoprotein particle binding
VEGF-activated receptor activity
KEGG
Leukocyte transendothelial migration
PPAR signaling
Fold
-log(P value)
F
GOMF
PDGF binding
IGF binding
KEGG
PI3K-Akt signaling
TGF-b signaling
G
Myogenesis
NES: 1.623
FDR: 0.021
TGF-b signaling
NES: 1.468
FDR: 0.072
Enrichment score
H
MSC markers
Ly6a
Mcam
Cspg4
Kit
Tbx18
Adam12
Pdgfa
Cd44
Pdgfrb
Cd34
Pdgfra
I
Cd34
p = 0.0005
Cd44
p = 0.0001
Pdgfrb
p = 0.0001
Pdgfra
p = 0.0351
Log2(counts)

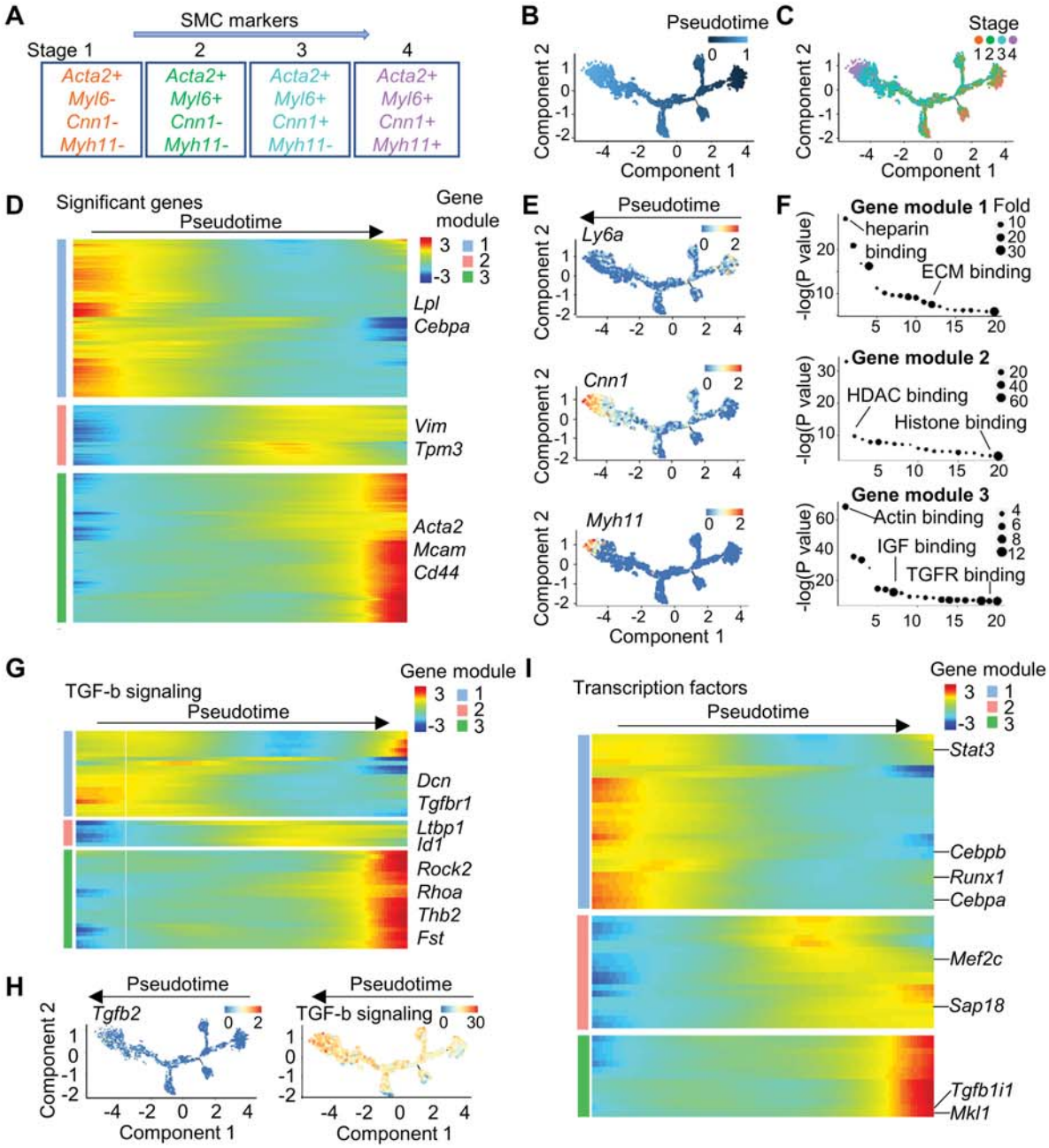
A
SMC markers
Stage 1
2
3
4
Acta2+ Myl6- Cnn1- Myh11-
Acta2+ Myl6+ Cnn1- Myh11-
Acta2+ Myl6+ Cnn1+ Myh11-
Acta2+ Myl6+ Cnn1+ Myh11+
B
Pseudotime
Component 2
Component 1
C
Stage
1 2 3 4
D
Significant genes
Pseudotime
Gene module
Lpl
Cebpa
Vim
Tpm3
Acta2
Mcam
Cd44
E
Pseudotime
Ly6a
Cnn1
Myh11
F
Gene module 1
heparin binding
ECM binding
Gene module 2
HDAC binding
Histone binding
Gene module 3
Actin binding
IGF binding
TGFR binding
-log(P value)
Fold
G
TGF-b signaling
Dcn
Tgfbr1
Ltbp1
Id1
Rock2
Rhoa
Thb2
Fst
H
Tgfb2
TGF-b signaling
I
Transcription factors
Stat3
Cebpb
Runx1
Cebpa
Mef2c
Sap18
Tgfb1i1
Mkl1

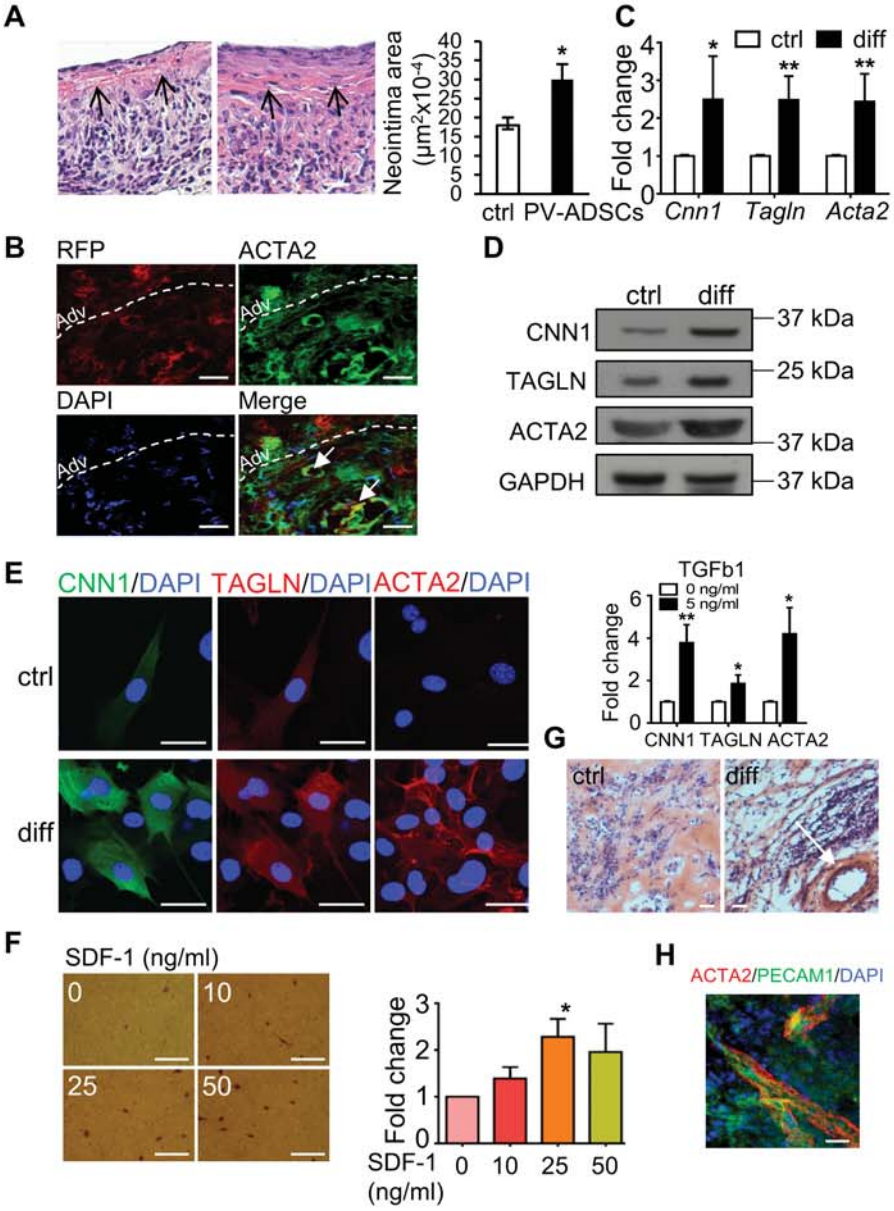
A
Neointima area (μm²x10⁻⁴)
ctrl
PV-ADSCs
C
ctrl
diff
Fold change
Cnn1
Tagln
Acta2
B
RFP
ACTA2
DAPI
Merge
Adv
D
ctrl
diff
CNN1
TAGLN
ACTA2
GAPDH
37 kDa
25 kDa
37 kDa
37 kDa
E
CNN1/DAPI
TAGLN/DAPI
ACTA2/DAPI
ctrl
diff
TGFb1
0 ng/ml
5 ng/ml
Fold change
CNN1 TAGLN ACTA2
G
ctrl
diff
F
SDF-1 (ng/ml)
0
10
25
50
Fold change
SDF-1 (ng/ml)
H
ACTA2/PECAM1/DAPI

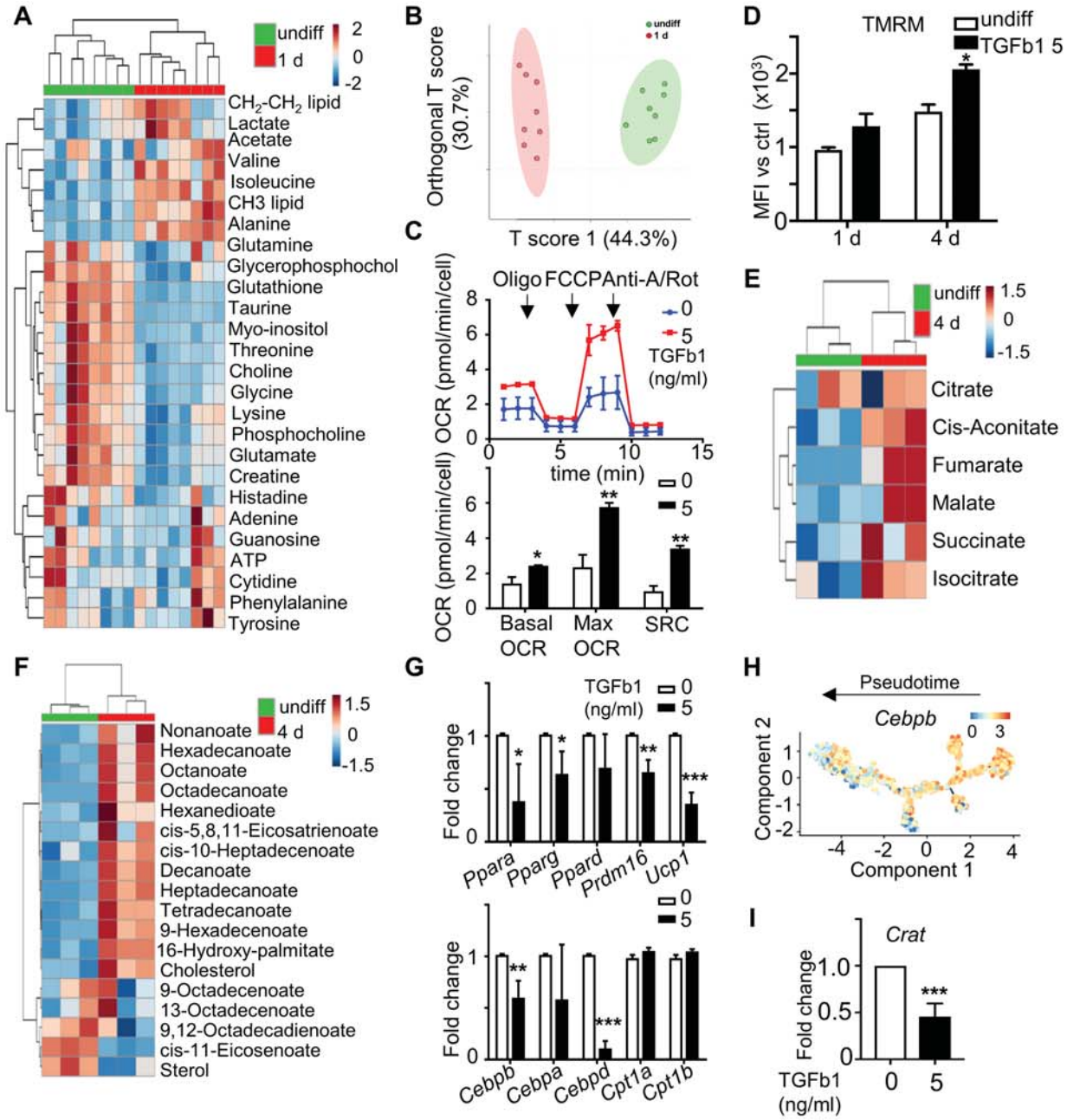
A
undiff
1 d
2
0
-2
CH2-CH2 lipid
Lactate
Acetate
Valine
Isoleucine
CH3 lipid
Alanine
Glutamine
Glycerophosphochol
Glutathione
Taurine
Myo-inositol
Threonine
Choline
Glycine
Lysine
Phosphocholine
Glutamate
Creatine
Histadine
Adenine
Guanosine
ATP
Cytidine
Phenylalanine
Tyrosine
B
Orthogonal T score (30.7%)
T score 1 (44.3%)
C
Oligo FCCP Anti-A/Rot
OCR (pmol/min/cell)
time (min)
TGFb1 (ng/ml)
0
5
Basal OCR
Max OCR
SRC
D
TMRM
undiff
TGFb1 5
MFI vs ctrl (x10^3)
1 d
4 d
E
undiff
4 d
1.5
0
-1.5
Citrate
Cis-Aconitate
Fumarate
Malate
Succinate
Isocitrate
F
undiff
4 d
1.5
0
-1.5
Nonanoate
Hexadecanoate
Octanoate
Octadecanoate
Hexanedioate
cis-5,8,11-Eicosatrienoate
cis-10-Heptadecenoate
Decanoate
Heptadecanoate
Tetradecanoate
9-Hexadecenoate
16-Hydroxy-palmitate
Cholesterol
9-Octadecenoate
13-Octadecenoate
9,12-Octadecadienoate
cis-11-Eicosenoate
Sterol
G
TGFb1 (ng/ml)
0
5
Fold change
Ppara
Pparg
Ppard
Prdm16
Ucp1
Cebpb
Cebpa
Cebpd
Cpt1a
Cpt1b
H
Pseudotime
Cebpb
0
3
Component 2
Component 1
I
Crat
Fold change
TGFb1 (ng/ml)
0
5

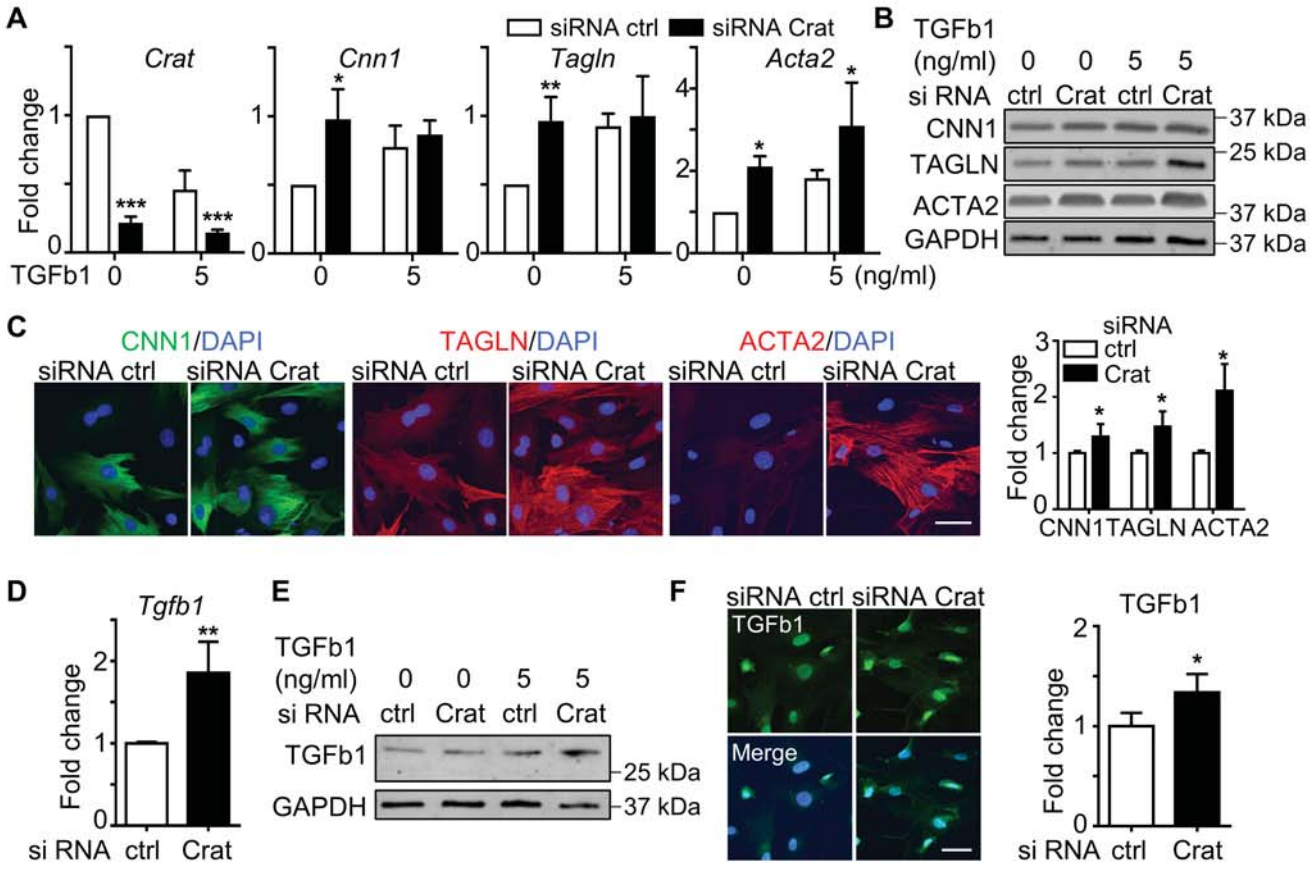
A
siRNA ctrl
siRNA Crat
Crat
Cnn1
Tagln
Acta2
Fold change
TGFb1 0 5
0 5
0 5
0 5 (ng/ml)
B
TGFb1 (ng/ml) 0 0 5 5
si RNA ctrl Crat ctrl Crat
CNN1
TAGLN
ACTA2
GAPDH
37 kDa
25 kDa
37 kDa
37 kDa
C
CNN1/DAPI
TAGLN/DAPI
ACTA2/DAPI
siRNA ctrl
siRNA Crat
siRNA
ctrl
Crat
Fold change
CNN1 TAGLN ACTA2
D
Tgfb1
Fold change
si RNA ctrl Crat
E
TGFb1 (ng/ml) 0 0 5 5
si RNA ctrl Crat ctrl Crat
TGFb1
GAPDH
25 kDa
37 kDa
F
siRNA ctrl siRNA Crat
TGFb1
Merge
TGFb1
Fold change
si RNA ctrl Crat

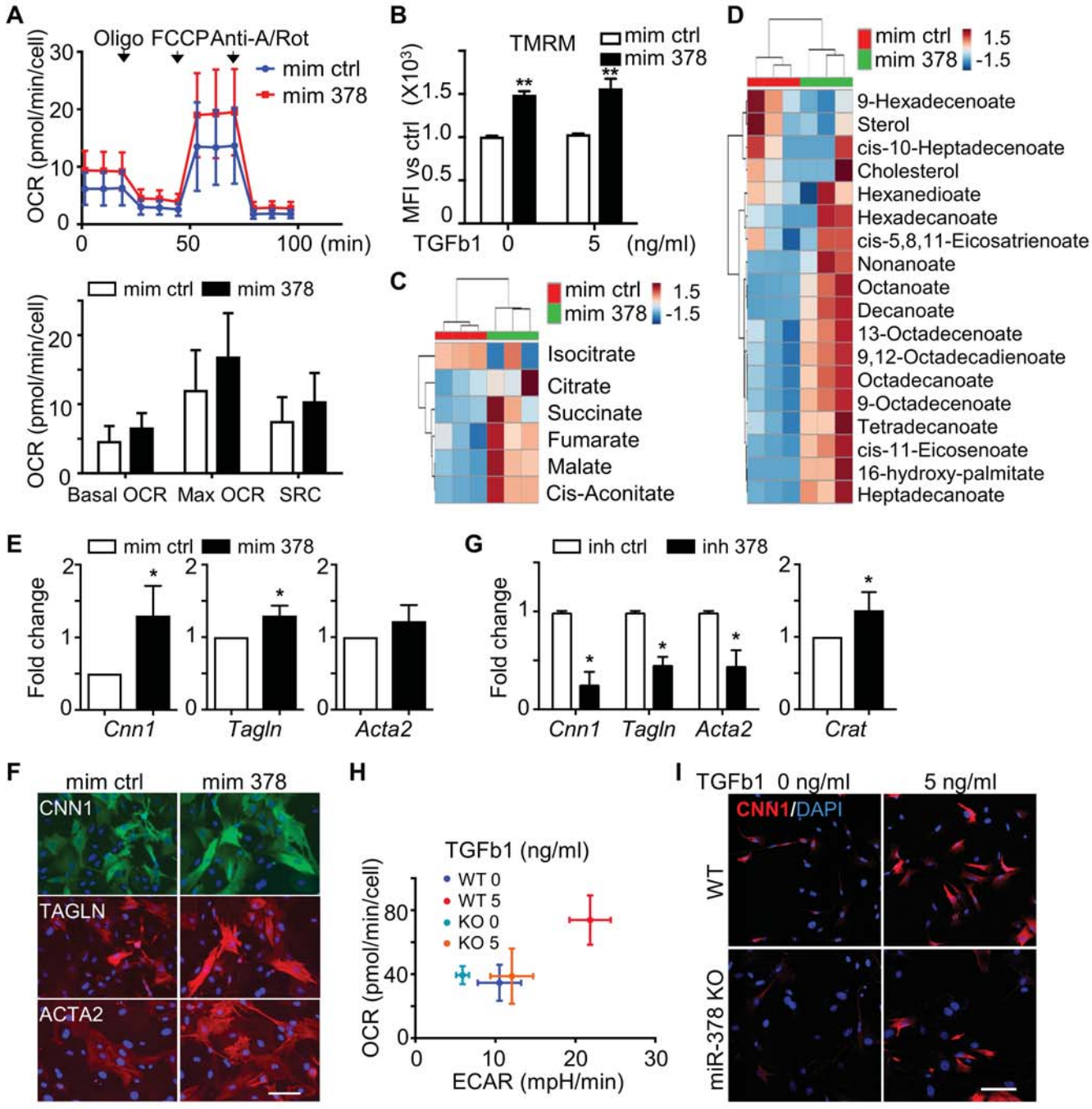
A
Oligo FCCP Anti-A/Rot
mim ctrl
mim 378
OCR (pmol/min/cell)
30
20
10
0
0
50
100 (min)
mim ctrl
mim 378
OCR (pmol/min/cell)
20
10
0
Basal OCR
Max OCR
SRC
B
TMRM
mim ctrl
mim 378
MFI vs ctrl (X10^3)
1.5
1.0
0.5
0
**
**
TGFb1 0
5 (ng/ml)
C
mim ctrl
mim 378
1.5
-1.5
Isocitrate
Citrate
Succinate
Fumarate
Malate
Cis-Aconitate
D
mim ctrl
mim 378
1.5
-1.5
9-Hexadecenoate
Sterol
cis-10-Heptadecenoate
Cholesterol
Hexanedioate
Hexadecanoate
cis-5,8,11-Eicosatrienoate
Nonanoate
Octanoate
Decanoate
13-Octadecenoate
9,12-Octadecadienoate
Octadecanoate
9-Octadecenoate
Tetradecanoate
cis-11-Eicosenoate
16-hydroxy-palmitate
Heptadecanoate
E
mim ctrl
mim 378
Fold change
2
1
0
*
*
Cnn1
Tagln
Acta2
G
inh ctrl
inh 378
Fold change
2
1
0
*
*
*
*
Cnn1
Tagln
Acta2
Crat
F
mim ctrl
mim 378
CNN1
TAGLN
ACTA2
H
TGFb1 (ng/ml)
WT 0
WT 5
KO 0
KO 5
OCR (pmol/min/cell)
80
40
0
0
10
20
30
ECAR (mpH/min)
I
TGFb1 0 ng/ml
5 ng/ml
CNN1/DAPI
WT
miR-378 KO